College of Science, Health, Engineering and Education
Chemical and Metallurgical Engineering and Extractive Metallurgy
www.murdoch.edu.au

Pilot Studies for Intermittent Dynamic Electrowinning using Renewable Energy

Final Report

19 October 2021

Element 25
Ian Huitson

Murdoch University
Associate Professor Aleks Nikoloski Dr
Touma B. Issa
Mr Allan Ang
Mr Mitchell Walker

This Project received funding from ARENA as part of ARENA's Advancing Renewables Program. The views expressed herein are not necessarily the views of the Australian Government, and the Australian Government does not accept responsibility for any information or advice contained herein.

Project overview and status

Project Summary

In early 2019, Element 25 Ltd (**E25**) approached ARENA and was awarded a grant to cover a project to determine the applicability of the use of renewable energy within the production of Electrolytic Manganese Metal (**EMM**). This program, Pilot Studies for Intermittent Dynamic Electrowinning using Renewable Energy, was approved utilising Murdoch University (**Murdoch**) as the research partner.

The project was proposed in 3 phases:

Phase 1, was conducted in two parts:

- Part A) Was the determination of optimal EMM electrolytic operating parameters in a laboratory environment; &
- Part B) Was the determination of the impacts that power supply fluctuations both positive and negative had on the electrowinning process.

Phase 2, Was the collection of 12 months of solar radiance and wind data from the Butcherbird Mine site. This work happened concurrently with Phase 1.

Phase 3, was to be a full-scale evaluation of the production of EMM using the real-world power supply based on results of Phase 2 data

Phase 1 was completed successfully and demonstrated that high grade (>99%Mn) EMM could be produced from the Butcherbird manganese ores. During Phase 1, Murdoch observed that often the EMM produced was not able to be easily removed from the cathodes following electrolysis.

To this end Murdoch proposed a change to Phase 3, in that

a) The first part of Phase 3 would be utilised to research and evaluate cathode pre-treatment methods &
b) The second part of Phase 3 be reduced to utilize a ¼ scale cathode (0.5m x 0.5m) for which Murdoch had an existing cell.

Phase 2 comprising the collection of 12 months of Solar Radiance and Wind data was completed shortly after the completion of Phase 1, a summary of results is shown at:
https://www.element25.com.au/site/sustainability/renewables

Phase 3 part a) was undertaken during the first half of 2020. In March 2020, all work at Murdoch stopped due to Covid-19 restrictions. Work on the project did not resume until June/July 2020 and work on Phase 3 part a) was completed in Aug 2020. The results of Phase 3 part a) showed that there are a number of pre-treatment options including both physical preparation of the cathodes as well as chemical treatments that assisted in the removal of the manganese from the cathodes. This is summarized in the following report.

During this same period, Element 25 had completed an internal economic study into the production of EMM (**Study**). The internal study, which is unpublished, highlighted a number of opportunities for the company to change the development strategy and focus for the Butcherbird Manganese project. Opportunities identified during the Study highlighted that the production and sale of manganese concentrate in the 30-35% Mn range was now viable.

As such E25 diverted resources to the implementation of the manganese concentrate business. Resulting in the redeployment of resources away from the EMM work being undertaken at Murdoch.

During the first half of 2020 Element 25 completed and published a PFS document defining the development of a manganese concentrate business at Butcherbird. This marked the change from the direct development of a an EMM mine and production facility to the organic growth of the Butcherbird project via the Manganese Concentrate, High Purity Manganese Sulphate (**HPMSM**) and eventually EMM pathway.

Murdoch was advised that the project was being halted at the conclusion of Phase 3, part a).

The Murdoch report below is the Project Summary document detailing the completion of work up to Phase 3, Part a). Please see details below.

College of Science, Health, Engineering and Education
Chemical and Metallurgical Engineering and Extractive Metallurgy
www.murdoch.edu.au

Progress Report 1/3

ARENA PHASE 3: Manganese Process Development Study

25 November 2020

Associate Professor Aleks Nikoloski
Dr Touma B. Issa
Mr Allan Ang
Mr Mitchell Walker

Metallurgical Process Research Development and Innovation Group
Murdoch University

Contents

Executive Summary iv

List of Figures v

List of Tables vii

1 Background 1

2 Aims and Objectives 1

3 Literature Review 2

3.1 Electropolishing 2

3.1.1 Mechanism of electropolishing 3

3.1.2 Potential and current density 4

1.1.1. Temperature 4

1.1.2. Electrolyte composition 5

1.1.3. Electropolishing duration 6

4 Results and Discussion 7

4.1 Electropolishing 7

4.1.1 Scope of work 7

4.1.2 Mechanical polishing and alternative methods 7

4.1.3 Electropolishing preliminary test (P3S5-1) 10

4.1.4 Electropolishing preliminary test (P3S5-2) 13

4.1.5 Electropolishing reactor 14

4.1.6 Electropolishing preliminary test (P3S5-3) 15

4.1.7 Electropolishing using formula used in China electrolyte 16

4.1.8 Linear sweep voltammetry 17

4.2 Electrowinning Tests 21

4.2.1 4-hour test 21

4.2.2 24-hour test 23

4.2.3 Deportment of selenium in 4-hour test 24

4.2.4 SEM-EDX report of unknown black substance 27

4.3 Pilot Plant 35

4.3.1 Current cell arrangement 35

4.3.2 Proposed cell modifications 37

4.3.3 Proposed electrodes 40

4.3.4 Diaphragms 42

4.3.5 Overall electrolyte circulation 42

5 Conclusions 43
6 References 44

Executive Summary

Scope

This document is reporting the main outcomes of the ARENA Phase 3 project after the first third of the overall project. It comes as a semi-final report in addition to the monthly interim reports. The main activities during this last two-month reporting period were focussed on the following three items:

i. Pre-treatment process for the Stainless Steel (SS) cathodes to prevent fusing of EMM on the substrate

ii. Polishing process of the SS cathodes for periodic maintenance following plating to enable multiple electrowinning plating cycles without much deterioration in EMM deposit quality.

iii. Design and fabrication of a Pilot Plant for demonstration of the integrated EMM electrowinning process

Findings

The investigation of pre-treatment process options showed that electropolishing is a preferred option. An effective process procedure has been developed by which smooth plated metal surface can be obtained. Several parameters that affect the metal surface like electrolyte, current density, temperature, and potential were tested during this project. Data from the two electrowinning tests were consistent with the results from Phase 1 and 2, but the EMM deposit from the 24-hour electrowinning test was noticeably black around its edges especially the region nearest to the solution line. The results from the SEM-EDX characterisation of the black powdery compound appear to suggest it as some sort of oxides, possibly of manganese, consistent with the results from the SEM-EDX characterisation of the black region on the metal piece. Trace amount of cobalt was detected on the surface, which in some past studies has been related as possible cause for black appearance on EMM deposits, which may require some additional study. A full design to prepare a pilot plant for the manganese electrowinning has been developed. The design included the dimensions of the EW cell and cathode and also the flow of electrolyte through the cell in its current state.

Recommendations

The project has been progressing well, as planned up to this point. The findings to date have been positive and certainly merit additional future work. It is recommended to proceed with the remainder of the ARENA funded Phase 3 project at an agreed future time between Element 25 and ARENA. Possible further developments in the scoped activities can be made based on the learnings from the work completed to date.

Associate Professor Aleks Nikoloski

Academic Chair of Extractive Metallurgy

List of Figures

Figure 1 Typical setup of the electrolytic cell for electropolishing 3
Figure 2: Comparison of mass transport mechanisms (a) salt film model and (b) acceptor species model [5] 3
Figure 3- A current-voltage curve showing the etching, passivating, polishing and pitting regions [8] 4
Figure 4 – The current density-voltage curves of 316L stainless steel at varying temperatures using 1:1 ratio of phosphoric and sulphuric and a rotating cylinder electrode at 3500 rpm [10] 5
Figure 5: Effect of electropolishing time on surface roughness [12] 6
Figure 6 Manganese deposits on the same SS cathode, showing significant quality attenuation with increasing number of plating cycles. From left to right, 1st test, 2nd test and 3rd test deposits 8
Figure 7: Experimental setup for electropolishing preliminary test (P3S5-1) 10
Figure 8: Cathode from P2S4-18 before (left) and after polishing (right) 11
Figure 9: Cathode from P2S4-18 before (left) and after polishing (right) using a 40x magnification 11
Figure 10: Yellow/brown colour change seen in electrolyte during electropolishing 12
Figure 11: New bushed SS cathode before (left) and after polishing (right) 13
Figure 12: Temperature control vessel showing PVC construction, and water inlet (bottom right) and outlet (top left) which water is circulated through via a heat exchanger 14
Figure 13: Electropolishing setup showing the inner PVC acid containment vessel where electropolishing takes place, and outer PVC water jacket, which water is pumped through using a Grant 1.5 kW heater 15
Figure 14: Cathode before (left) and after polishing in test (P3S5-3) (right). Both images are 40x zoom 16
Figure 15: Comparison of electropolishing experiment 2 and 3 performed on a brushed 316 stainless steel electrode 16
Figure 16: Linear sweep scan of electropolishing solution formula used in China using a 304/304L dual grade stainless steel anode and 316 stainless steel cathode. The scan rate was 1 mV/s 18
Figure 17: Photo of 304 after polishing at 400 A/m^2 (top) and images under the microscope of the inner dull areas (bottom left) and outer more polished sections (bottom right) 19
Figure 18: Microscope images of regular and low light (top left and middle), and images of the polished electrode (bottom and right) 20
Figure 19: Stainless steel polished using Chinese electrolyte and 5V 21
Figure 20: Current density and potential readings for the 4-hour manganese electrowinning test 22
Figure 21: Catholyte pH over the 4-hour test 22
Figure 22: Manganese deposit on 304 stainless steel cathode after 4-hour of electrowinning 22
Figure 23: Current density and cell potential over the duration of the 24-hour manganese EW test 23
Figure 24: Anolyte and catholyte pH over the 24-hour manganese EW test 23
Figure 25: Manganese deposit from the 24-hour test 24
Figure 26. Black regions seen on edges of EMM deposit from 24-hour electrowinning test 28
Figure 27. Metal piece placed on SEM stub using a carbon tape before mounted on SEM instrument 28
Figure 28. Normalised EDX spectra of spot analyses and area scan of unknown black powdery compound 29
Figure 29. Metallic region of metal piece under SEM backscattered imaging 31
Figure 30. EDX area scan of metallic region of metal piece 31
Figure 31. Morphological structure of metal piece 32
Figure 32. Black region of metal piece under SEM backscattered imaging 32
Figure 33. Normalised EDX spectra of spot analyses and area scan of the darker area (middle of Figure 32) 33

Figure 34. Normalised EDX spectra of spot analyses and area scan of black region of metal piece 34
Figure 35: Current EW cell inside dimensions 35
Figure 36: Side view of current EW cell showing feed inlet and overflow weir 36
Figure 37: Current EW cell cathode dimensions.....36
Figure 38: Outside dimensions of the pre-existing cell, showing the proposed smaller cell, which would be placed inside the larger cell. Note for simplicity the diaphragm boxes are not included in this diagram 37
Figure 39: Proposed cell dimensions for the smaller cell, which will house the anodes and cathodes during operation 38
Figure 40: Inlet and outlet of small inner cell.....39
Figure 41: Cross sectional diagram of proposed cell configuration.....40
Figure 42: Top view of cell configuration, showing feed manifold (green) 40
Figure 43: Cathode size for EMM EW cell.....41
Figure 44: Anode design 1; same length and smaller width..... 41
Figure 45: Anode design 2; perforated anode of the same length and width as the cathodes 42
Figure 46: Overall circulation of the electrolyte of the pilot plant 43

List of Tables

Table 1 Polishing Methods....2
Table 2 Cathode *Pre-treatment* operating parameters....8
Table 3 Cathode Polishing operating parameters....9
Table 4 Cathode Polishing electrolyte compositions....9
Table 5 Preliminary test (P3S5-1) variables....12
Table 6 Preliminary test 2 variables....13
Table 7 Preliminary test P3S5-3 variables....15
Table 8: Suppliers contacted....17
Table 9: Comparison of 304 stainless steel composition....17
Table 10: Electropolishing test parameters for P3S5-4. 18
Table 11: Electropolishing test parameters for P3S5-5 19
Table 12: Electropolishing test parameters for P3S5-6 20
Table 13: Electrolyte analysis performed at MARINE (78SE)....25
Table 14: Accountability from MARINE 25
Table 15: Mass percentages MARINE....26
Table 16 Selenium NAGROM 82SE 26
Table 17 Accountability from NAGROM 27
Table 18 Selenium MURDOCH 80 SE 27
Table 19 Accountability from Murdoch....27

1 Background

Element 25 is a Western Australian company seeking assistance to develop a novel and economic process to produce high purity manganese products from its Butcherbird Manganese Deposit, which hosts Australia's largest onshore manganese resource [1] comprising > 180 Mt of near surface manganese oxide ore. The process should be suitable to produce electrolytic manganese metal (EMM), but also high purity manganese sulphate (MS) and electrolytic manganese dioxide (EMD). The recently completed scoping study (ARENA Phase 1) and process optimisation study (ARENA Phase 2) have returned robust results and a Pre-Feasibility Study has been initiated to progress the Project. The next stage of the process development should further optimise the EMM production process and products quality, provide information that will maximise the utilisation of energy by integrating innovative applications of renewable energy sources and to demonstrate this on a pilot plant scale.

Following the excellent results from the ARENA Phase 1 and Phase 2 projects on the development and optimisation of technology to produce electrolytic manganese metal, the present phase of process development work of the continuing ARENA project is Phase 3 and this report summarises the development in first third of this work. The scope of the first third of the Phase 3 focused on the development of outstanding processes for the production of EMM, i.e.:

1. *Pre-treatment process* for the Stainless Steel (SS) cathodes to prevent fusing of EMM on the substrate
2. *Polishing process* of the SS cathodes for periodic maintenance following plating to enable multiple electrowinning plating cycles without much deterioration in EMM deposit quality.
3. *Design and fabrication of a Pilot Plant* for demonstration of the integrated EMM electrowinning process.

2 Aims and Objectives

The aim of the overall Phase 3 is to assess process parameters and reagent additions to increase the tolerance of IDE at lower current densities and carry out large scale testwork to validate and further develop an economic and novel process for the electrolytic manganese metal production for integration to renewable energy sources.

The study is flexible but the target main objectives are to:

1. Study the effects of pre-treatment process options to develop an effective pre-treatment of the SS cathodes which can effectively overcome the delamination and morphology issues observed in the previous phases of work.
2. Conduct experiments involving longer plating time and plating at lower current densities to develop an improved understanding of the effects of these two key parameters under critical conditions.
3. Arrange for the fabrication of suitable diaphragm(s) and complete the adaptation of the medium size pilot plant electrowinning cell(s) for EMM work.
4. Conduct medium size piloting test work to validate process for periods long enough to demonstrate steady operation
5. Identify aspects of concern and opportunities for further improvement.
6. Establish preliminary descriptions of optimal conditions for full scale IDE
7. Generate larger samples for detailed characterisation of the products
8. Consider factors affecting EMM morphology and stress formation.

3 Literature Review

Polishing can be defined as the process of making a surface smooth and or shiny. The methods of doing so can generally be categorized into one of the four following groups [2], although some research into using a combination of methods, such as mechanical chemical polishing has been conducted [3].

1. Mechanical
2. Electrical
3. Chemical
4. Electrochemical

The traditional method of polishing is mechanical, which consists of using an abrasive media, such as a sanding belt, grinding or buffing wheel. This method of polishing has the potential to leave imperfections and impurities on the surface of the polished item transferred from the abrasion source, which can affect the mechanical and electrical properties of the polished material. Therefore, electropolishing will be investigated as an alternative method of polishing.

Table 1 Polishing Methods

Method	Descriptions	Limitations
Mechanical	Polishing via physical abrasion, *e.g.*, buffing wheel or sand paper.	Leaves surface imperfections and impurities. Time consuming.
Electrical	High energy polishing, *e.g.*, plasma polishing.	Still largely in development stage. Not yet feasible for large scale operations.
Chemical	Polishing performed in a solution without any electricity.	Longer polishing times than electropolishing Higher surface roughness of polished specimen Not as prominent in literature
Electrochemical	Opposite process to electroplating. Polishes by applying a positive current to the work piece while submerged in electrolyte.	Optimal conditions vary largely depending on the system variables.

3.1 Electropolishing

Electropolishing is another type of electrolysis in which a direct electric current pass through an electrolyte in an electrolytic cell (Figure 1). The electropolished piece (anode) is connected to a positive terminal. During the electropolishing process the metal of the positive electrode (anode) is detached from the surface and turns into cations (positive ions), that move to the cathodic side. At the end of the process, the anodic surface becomes smoother.

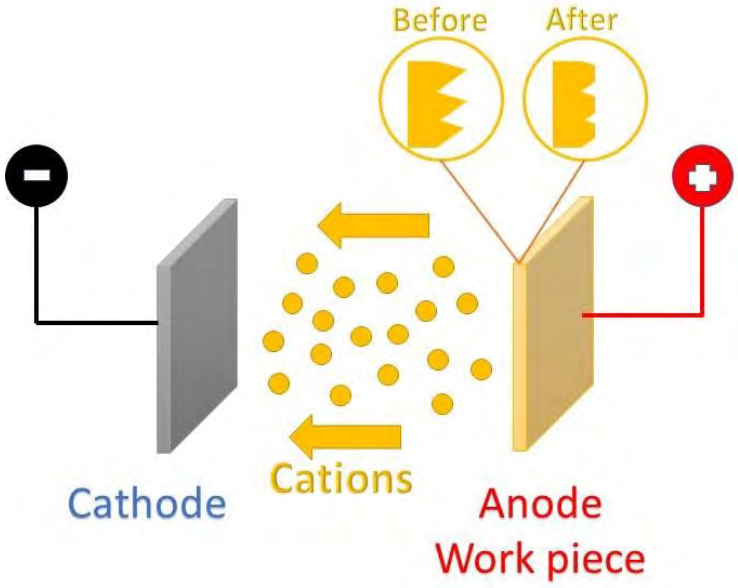

Figure 1 Typical setup of the electrolytic cell for electropolishing.

3.1.1 Mechanism of electropolishing

The two electropolishing theories present in literature are the salt film mechanism and the acceptor mechanism [4-7]. In the salt film mechanism, the rate limiting step is the transport of dissolving metal ions from the anode surface to the bulk electrolyte. At the anode electrolyte interface, there is a thin salt film formed by the reaction between dissolving metal ions and electrolyte anions. Therefore, the dissolution of metal ions from the anode is limited by the saturation concentration in the salt film. The current is therefore constant once the saturation concentration is reached.

In the acceptor mechanism, the rate determining step is the transport of acceptor species in the electrolyte such as complexing anions or water is limiting. The dissolving metal ions react with the water or complexion anions to form complexed or hydrated species. As they react at the anode electrolyte interface, the concentration of the acceptor species is reduced until the concentration is zero. This corresponds to the limiting current.

The differences between the two mechanisms can be shown via the diagram in Figure 2.

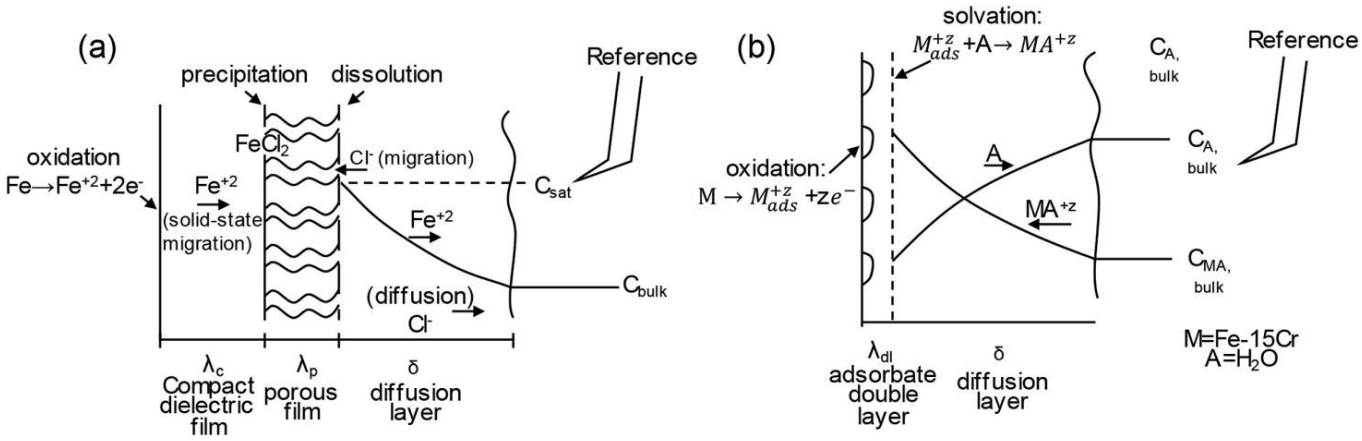

Figure 2: Comparison of mass transport mechanisms (a) salt film model and (b) acceptor species model [5]

3.1.2 Potential and current density

The effect of varying potential and resulting current can be understood by studying a current-voltage curve, such as the one shown in Figure 3. There are four different zones; etching, passivating, polishing and pitting. Etching occurs at the lowest potentials, and is where the anode is directly dissolved [8]. Pitting can occur in this region if the work piece has been mechanically worked. The passivating region shows a drop in current density, as there is an oxide layer that has built up, passivating the surface. In the polishing region, the passive layer is stabilised and dissolved species from the metal surface diffuse through the passivated layer [8]. In the pitting region, the passivated layer breaks down with increased potential and oxygen gas begins to form. The gas bubbles on the surface of the anode cause pitting, hence the name of this region.

For electropolishing, the applied potential should be within the polishing region of the current-voltage graph. Common voltage ranges in one literature source suggest 6 – 18V although it is noted that not all numbers within this range are economical [6].Another source however provided current voltage curves suggesting the ideal polishing potential to be 1.5 – 2.0V [9]. The ideal potential for electropolishing a material can be found by cycling the intended anode material on a potentiostat to obtain the current-voltage curve [5].

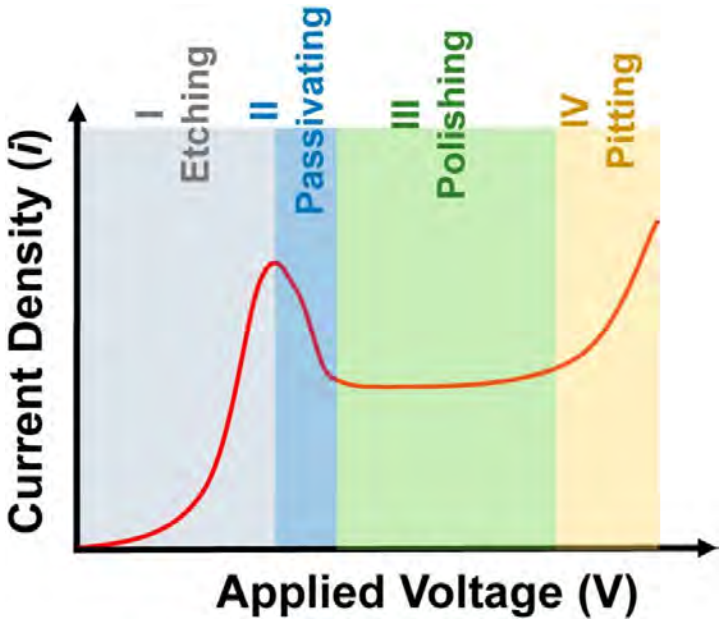

Figure 3- A current-voltage curve showing the etching, passivating, polishing and pitting regions [8]

The current density observed during the plateau within the polishing region is directly related to the polishing intensity. A higher current density is indicative of a greater anode dissolution rate. This can be problematic because with higher dissolution rate, the electrolyte contamination rate also increases. The ideal parameters would give a smooth surface while remove as little metal as possible.

1.1.1. Temperature

The temperature of the electrolyte is directly related to the mass transport of acceptor ions to and metal ions from the metal surface. At a lower temperature, the diffusion of ions is slower as the solution is more viscous. In addition, the solubility of metal ions is lowered, subsequently reducing the current density observed. At higher temperatures, the electrolyte is less viscous, allowing constant fresh electrolyte to contact the anode, preferentially dissolving the protruding surfaces.

Chen et al. [10] tested the effect of temperature on 316L stainless steel in various ratios of phosphoric and sulphuric acid using a rotating cylinder electrode at 3500rpm. It was discovered at a ratio of 1:1 H_3PO_4 to H_2SO_4 ,an increase in current density was observed when increasing the electrolyte temperature from 60 to 80 ^oC (Figure 4).This was supported by Eliaz and Nissan [11], who observed similar and also stated that although a higher temperature increases current density, the lowest temperature that provides good electropolishing can be chosen. Notably, an increase in phosphoric acid also increased the current density, suggesting the transport of HPO_4^- could be the limiting acceptor species at these conditions. The optimal temperature in terms of electropolishing finish was found to be 70^oC using a 1:1 ratio of phosphoric and sulphuric, however this was performed using porous stainless steel 316L so results may vary when using other steels

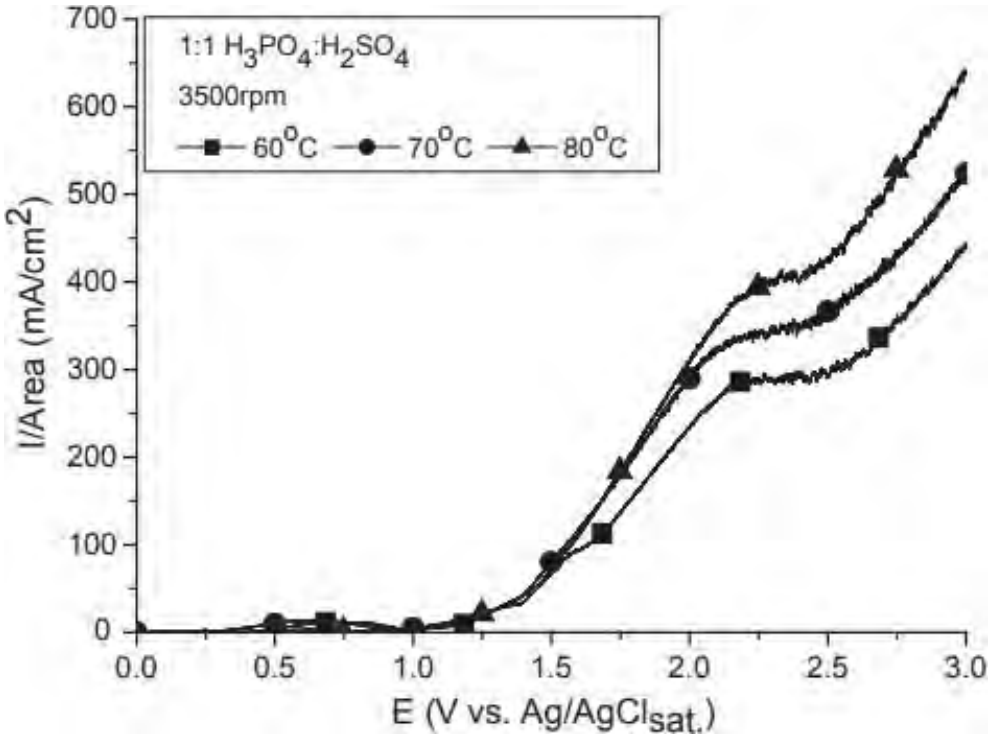

Figure 4 – The current density-voltage curves of 316L stainless steel at varying temperatures using 1:1 ratio of phosphoric and sulphuric and a rotating cylinder electrode at 3500 rpm [10]

1.1.2. Electrolyte composition

The electrolyte is the carrier of the current, and depending upon its properties, can directly impact the finish of the metal [5]. Ideal electrolytes must provide high quality surface finishes at low voltage and current density, while remaining stable whilst in operation and storage [6]. Favouring the formation of a viscous layer, promoting macroscopic levelling whilst being capable of dissolving the metal surface ions is another requirement [8].

The electrolyte composition depends heavily on the metal being polished. For example, copper shows better polishing with higher acid concentration however Nb-Ti alloys showed the opposite [5].

The most prevalent electrolyte composition in literature regarding stainless steel is varying ratios (1:1 – 1:3) of sulphuric acid and phosphoric acid. Additives such as glycerol and glycerine are popular choices when polishing 316 and 304 stainless steel [8]. Other, less common additives in literature are aniline and polyethylene glycol [8].

1.1.3. Electropolishing duration

The electropolishing duration was found to have a significant effect on surface roughness [12]. A polishing time of 6 minutes was found to significantly reduce the surface roughness, shown below in Figure5.

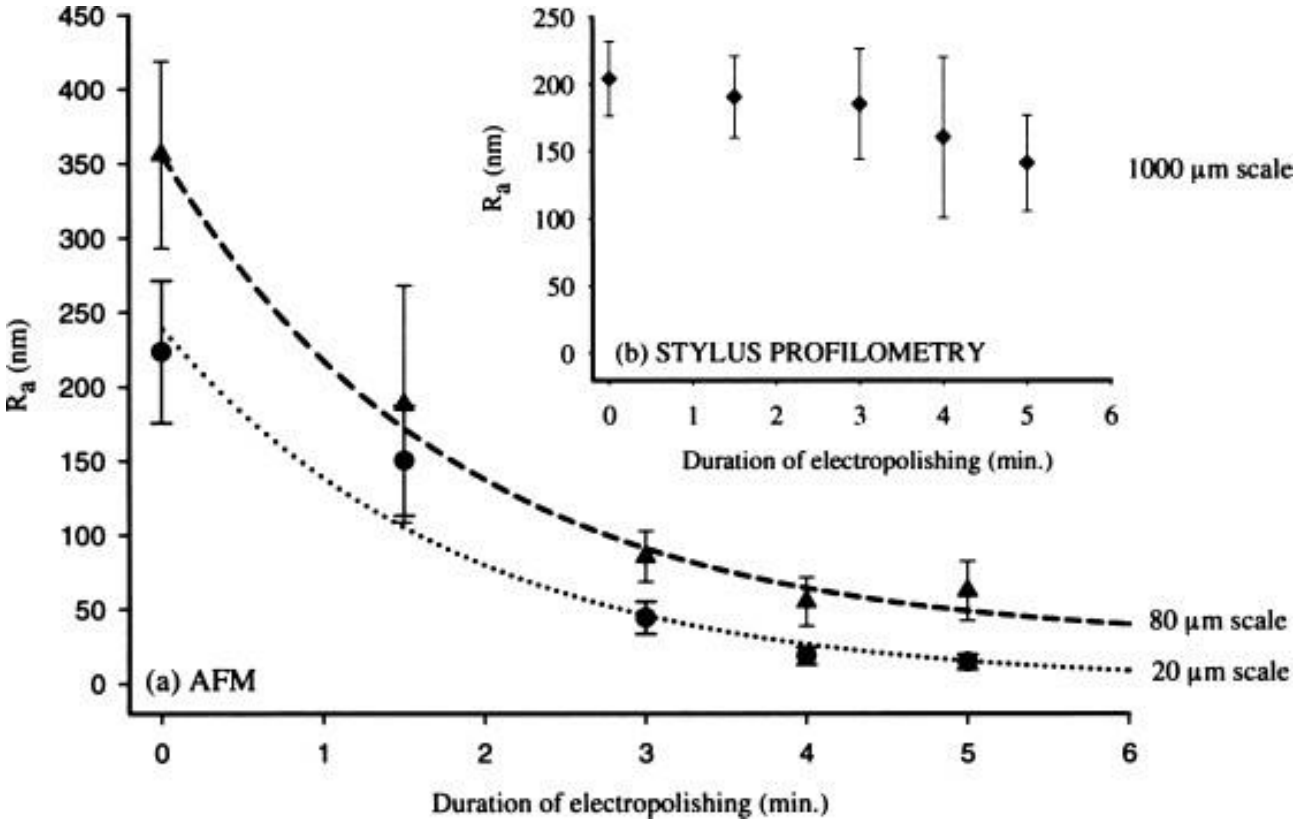

Figure 5: Effect of electropolishing time on surface roughness [12]

4 Results and Discussion

4.1 Electropolishing

4.1.1 Scope of work

This portion of the Phase 3 project will focus on the development of two important processes in the overall production of electrolytic manganese metal (EMM), namely:

1. *Pre-treatment* of the stainless steel (SS) cathodes to prevent fusing on the manganese metal onto the substrate – from here on referred to as Pro-treatment process; and

2. *Polishing* of the SS cathodes following plating to enable multiple electrowinning plating cycles without a significant deterioration in EMM deposit quality – from here on referred to as Polishing process.

Recall previously in phase 1 and 2, the SS electrodes were Pre-treated by dipping in a solution of sodium silicate before each electrowinning cycle. It was observed that the process can be optimised in terms of pre-treatment bath composition, duration of treatment and method of rinsing. Also, after the electrowinning and separation of the EMM deposit each electrode was subjected to mechanical Polishing before each test. It was noticed that there was a reduction in quality (illustrated in Figure 6) of the manganese metal deposits with successive plating onto the same SS substrate. This was assumed to be due to a change in the surface of the SS electrode surface which affects the quality of the deposit. The ideal Polishing procedure would return the SS surface to the effectively same state it was in before electrowinning took place.

The purpose of this segment of phase 3 research therefore is to formulate (i) an effective method of Pre-treatment and (ii) an alternative effective method of Polishing which will allow the same SS cathode to be reused multiple times, without a reduction in deposit quality.

4.1.2 Mechanical polishing and alternative methods

The initial method used for *Pre-treatment* was mechanical polishing, performed using 1200 grit silicon carbide sandpaper. Alternative approaches to this for polishing are chemical and electrochemical. Chemical methods involve immersing the substrate to be polished into a solution which dissolves the outermost layers, removing the constituents formed during the previous plating or harvesting cycle that have detrimental effect on the subsequent plating, and creating effectively a fresh surface.

Electrochemical *Polishing* methods on the other hand use electric current to oxidise the substrate and preferentially dissolve raised surfaces. It is believed that most of the existing EMM producers (mainly located in China) use electropolishing, therefore, testing procedure described in this report are focused on electropolishing. Preliminary information suggests that the polishing solutions are typically phosphoric/sulphuric acid mixture of different concentrations. This and also the required frequency and duration of electropolishing are subjects of the investigation. The effectiveness of the tested methods will be verified using nominally 15 g/L Mn catholyte such that the tests are aligned with the proposed plant design operating conditions, over a 24 hr plating cycle time.

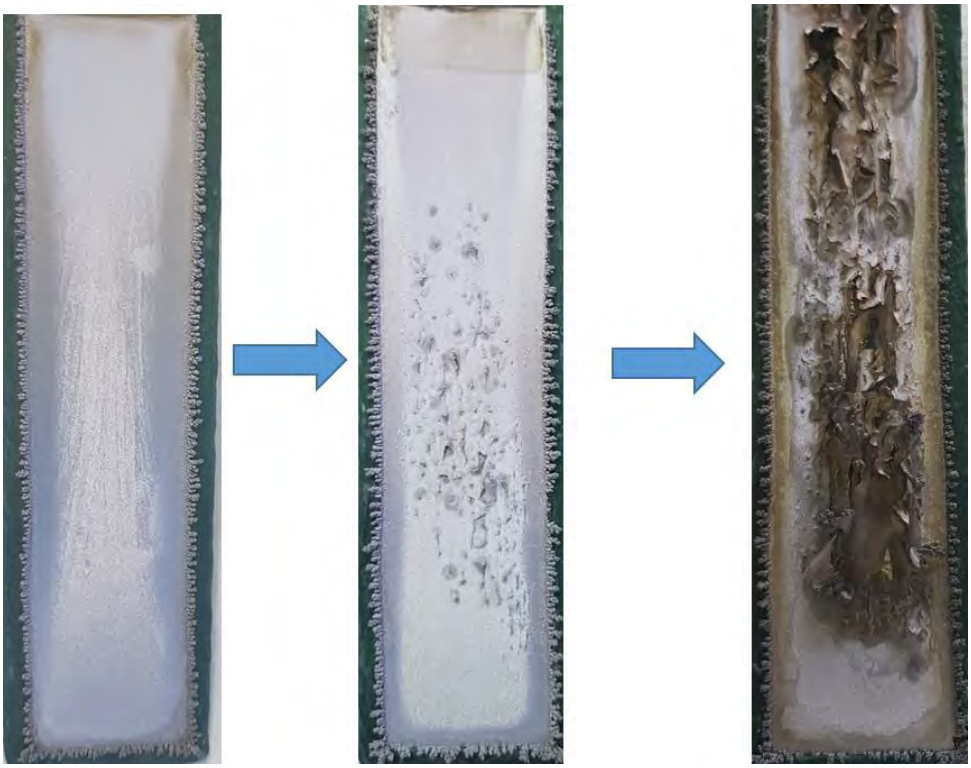

Figure 6 Manganese deposits on the same SS cathode, showing significant quality attenuation with increasing number of plating cycles. From left to right, 1st test, 2nd test and 3rd test deposits.

The baseline starting parameters for the development program for *Pre-treatment* and *Polishing* processes will consider information available in the literature, existing experience of the research staff and information based on Chinese experience summarised in the following two tables.

Table 2 Cathode *Pre-treatment* operating parameters

Sodium silicate solution	
	○ **Nominally 2% sodium silicate**
	○ **pH 7-8 adjusted with sodium hydroxide to maintain in target range**
Cycle times	
	○ **Dip time 5-10 sec**
	○ **Dry time 5-10 minutes**
Other	○ **Post pre-treatment avoid contact with dust or other deleterious materials**
	○ **1st cycle sodium silicate dip is not normally necessary for a new cathode.**

On the bases of this, the testwork will begin with assessment of the following electrolyte compositions. The testwork will include assessment of the effect of ultrasound.

Table 3 Cathode Polishing operating parameters

Frequency of polishing
○ **1 in every 20 days**
Polishing solution (phosphoric acid/sulphuric acid with additives)
• **Composition:**
○ **Phosphoric acid/Sulphuric acid ratio 3:2 w/w based upon 85% phosphoric acid and 96%-98% sulphuric acid**
• **Additives:**
○ **Glucose @ 0.1% w/w total H_3PO_4/H_2SO_4**
○ **Tributyl phosphate can be added as an anti-foaming agent**
• **Life: Up to 6 months with regular top-up for physical losses**
Polishing conditions
○ **Time – 10 minutes**
○ **Temperature – 55-65 °C**
Electrical conditions
○ **Cathode-Anode separation – 10 cm**
○ **Current – 350-400 A/m²**
○ **Voltage – 5-7 V**

Table 4 Cathode Polishing electrolyte compositions

Electrolyte Constituents	Composition, vol.%
H_2SO_4	50 %
H_3PO_4	50 %
H_2SO_4	75 %
H_2O	25 %
H_2SO_4	73 %
Glycerol	20 %
H_2O	7 %
H_2SO_4	55 %
H_3PO_4	30 %
H_2O	15 %
Glycerol	59 %
H_2O	20 %
H_2SO_4	11 %
H_3PO_4	10 %
H_3PO_4	59 %
H_2SO_4	39 %
Glucose/dextrose	2 %
H_3PO_4	60 %
H_2SO_4	40 %

4.1.3 Electropolishing preliminary test (P3S5-1)

The aims of the initial test were the following;

1. Conduct preliminary assessment of the effect of variables reported in literature to ensure that we are able to be replicate those in our laboratory setup

2. Test whether there was any difference observed in the surface of the SS before and after electropolishing for 2 minutes.

This test was conducted in a polypropylene measuring cylinder that was modified to a suitable height. This was clamped, partially submerged in a 5 L beaker of DI water. The temperature of the water was controlled by the hotplate and attached temperature controller.

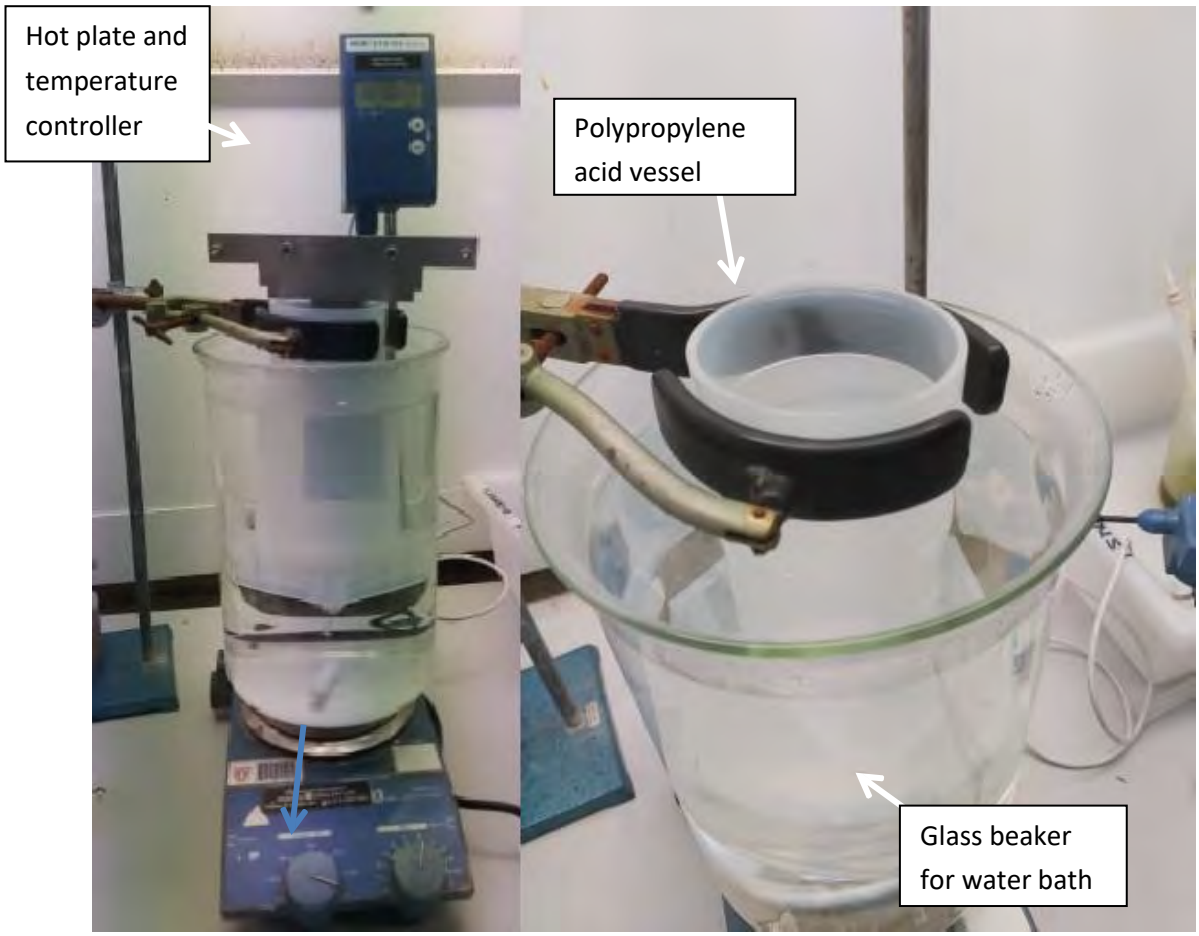

Figure 7: Experimental setup for electropolishing preliminary test (P3S5-1)

Images of the stainless steel before and after electropolishing can be seen in Figure 8. The initial 5 minutes consisted of immersing the SS in the electrolyte to assess whether any dissolution or polishing would occur without current. Some of the brown marks shown in the left image of Figure 8 were dissolving, however it was very slow. The current density was then raised to 0.15 A/cm^2 for 2 minutes of electropolishing. Following the polishing treatment, the surface of the electrode was cleaner and much shinier. The surface was not mirror finish, and the brushed marks were still visible (right image in Figure 9). There is evidence of surface change when the electrode is viewed under a Nikon LABOPHOT-POL optical microscope (Figure 9) The surface appears lighter, with the absence of some dark lines which were apparent before polishing. This could be due to the preferential dissolution

of the darker minerals in the metal, or to the increased reflection, creating an apparently brighter image when viewed through the microscope under the same light source.

Figure 8: Cathode from P2S4-18 before (left) and after polishing (right)

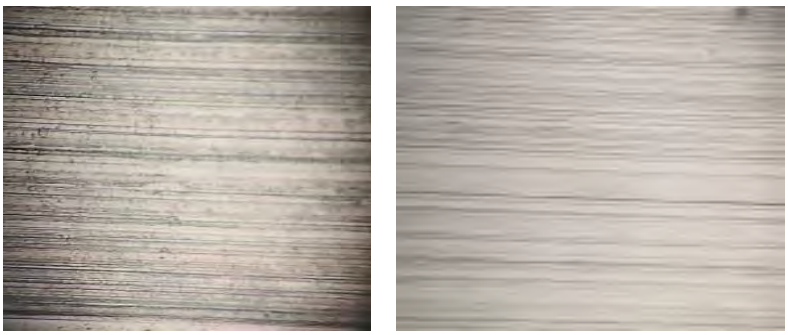

Figure 9: Cathode from P2S4-18 before (left) and after polishing (right) using a 40x magnification.

The electrolyte composition, temperature and current density for the initial test were based on ASTM B912 [13] and are summarised in Table 4.

Table 5 Preliminary test (P3S5-1) variables

Anode	The stripped cathode used in manganese electroplating test P2S4-18 (stainless steel with ultrasonic pre-treatment)
Cathode	Stainless steel cathode with stop-off paint used in the first stainless steel cathode EMM electroplating tests
Electrolyte composition	50/50 (v/v %) phosphoric acid (85%) and sulphuric (95%) **(batch 1)**
Time	5 minutes (no current) + 2 minutes (current applied)
Temperature (ºC)	~30°C (bath was 75ºC however acid wasn't given long enough to heat up)
Current	9 A (~0.15 A/cm^2)
Potential	8 V

Another potentially relevant observation made during this experiment was the colour change in the electrolyte. The electrolyte was initially colourless/ever so slightly yellow but turned to a dark orange/yellow/brown during electropolishing. This is shown in Figure 10 and is suspected to be due to dissolution products; possibly iron or chromium. A spot test with potassium thiocyanate solution gave a deep red colour solution, indicating the presence of iron. Literature [14, 15] claims the yellow colour could also be due to the presence of chromium (VI).

Figure 10: Yellow/brown colour change seen in electrolyte during electropolishing

4.1.4 Electropolishing preliminary test (P3S5-2)

The second test was carried out under the conditions specified in Table 5. The experiment setup used was identical to the first test (P3S5-1) (Figure 7). The aim of the test was to examine the following:

1. Establish rate of mass loss using a new brushed stainless-steel cathode
2. Test if polishing produces a more mirror-like finish.

Table 6 Preliminary test 2 variables

Anode	New brushed stainless steel
Cathode	Stainless steel cathode with stop-off paint used in the first stainless steel cathode EMM electroplating tests
Electrolyte composition	50/50 /v phosphoric acid (85%) and sulphuric (95%) **(batch 1)**
Time	2 minutes of applied current
Temperature (ºC)	~75 °C
Current	9 A (~0.15 A/cm^2)
Potential	8 V

Before the test began, the SS cathode weighed 98.67 g. Following 2 minutes of applied current, the cathode mass dropped to 98.52 g, indicating a mass loss rate of 75 mg/minute.

A comparison of the SS electrode before and after polishing can be seen in Figure 11. There is a visible uneven surface on the polished stainless electrode. This is believed to be the result of pitting. Pitting is due to the formation of oxygen gas on the anode surface, resulting in an uneven surface finish as the oxygen bubbles effect the local stainless steel dissolution rate.

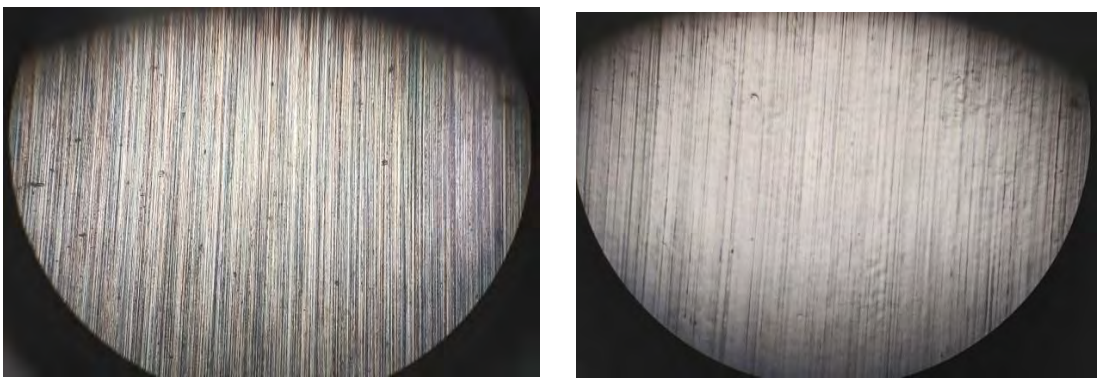

Figure 11: New bushed SS cathode before (left) and after polishing (right)

4.1.5 Electropolishing reactor

One problem made evident with the first two tests was the slow heating of the reaction vessel. It took more than 4 hours for the water bath and polishing solution to reach the desired temperature of 75°C. The long time required then to run the experiment prompted the design of a new vessel, which uses a PVC pipe and a laboratory bath circulator to provide heating instead of the glass beaker and hot plate used initially. The bath circulator was able to reach setpoint much quicker than the hot plate.

The heating vessel consists of a 100 mm diameter PVC pipe, with a cap glued on one end. Holes were cut at opposing sides of the pipe. One hole was cut at the bottom half of the pipe, and the other at the top. 15 mm PVC pipe was attached using PVC cement. Hoses were attached to these pipes with clamps and silicone, allowing water from the 1.5 kW Grant laboratory bath circulator to be pumped in from the bottom, and overflow out the top outlet. This vessel is shown in Figure 12.

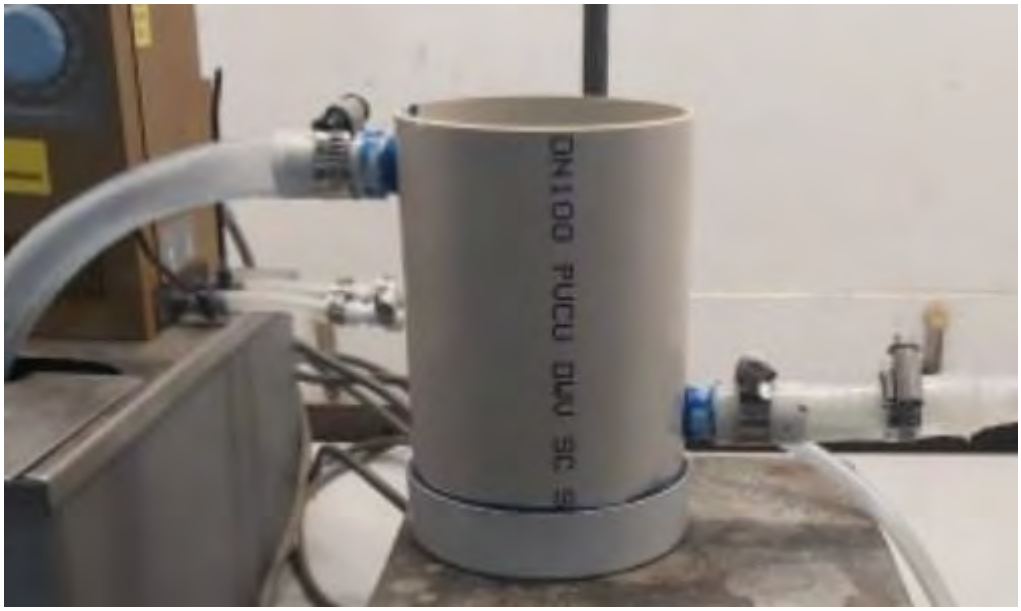

Figure 12: Temperature control vessel showing PVC construction, and water inlet (bottom right) and outlet (top left) which water is circulated through via a heat exchanger.

The reaction vessel is another PVC pipe, cut slightly longer and of a smaller (90mm) diameter. This pipe sits inside the larger vessel and contains the acid and holds the electrodes for polishing. Images of this can be seen in Figure 13. The polishing vessel is slightly taller than the temperature controlling outer PVC pipe in Figure 12, preventing the water from mixing with the acidic electrolyte.

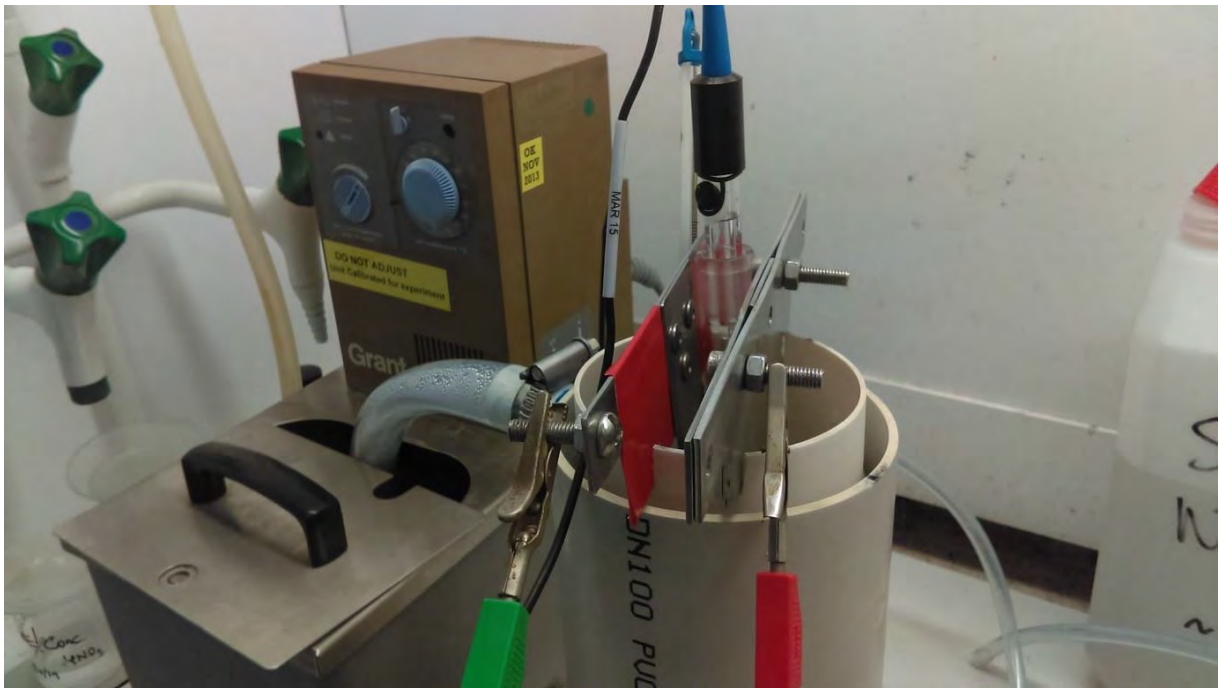

Figure 13: Electropolishing setup showing the inner PVC acid containment vessel where electropolishing takes place, and outer PVC water jacket, which water is pumped through using a Grant 1.5 kW heater.

4.1.6 Electropolishing preliminary test (P3S5-3)

The third test was conducted under slightly milder conditions, namely a reduction in polishing time to 1 minute. The aim was to see if the pitting on the cathode from the previous test could be minimised. The improved electropolishing setup described in Figure 12 Figure 13 was utilised for this test. The experimental conditions are summarised in Table 7.

Table 7 Preliminary test P3S5-3 variables

Anode	Brushed cathode used in EP test P3S5-2
Cathode	Stainless steel cathode with stop-off paint used in the first stainless steel cathode EMM electroplating tests
Electrolyte composition	50/50 /v phosphoric acid (85%) and sulphuric (95%) **(batch 1)**
Time	1 minute of applied current
Temperature (ºC)	~75 °C
Current	5.6 A (~0.15 A/cm^2)
Potential	5.0 V

Figure 14 shows the cathode under the optical microscope before and after polishing. The photo taken after polishing (right) clearly shows a more uneven surface. This is believed to be attributed to pitting.

A comparison of the tests P3S5-2 and P3S5-3, which were performed on the same electrode can be seen in Figure 15. Note the improved reflectivity of the cathode, as it approaches a more mirror like finish. At certain angles, the pitting is visible; however, this was unable to be captured by camera. One thing to note is, it isn't apparent how

smooth the cathode must be for manganese plating, so although pitting is not desired, it is possible it may not have a negative effect on the manganese deposit morphology. This will require further testing to form conclusions.

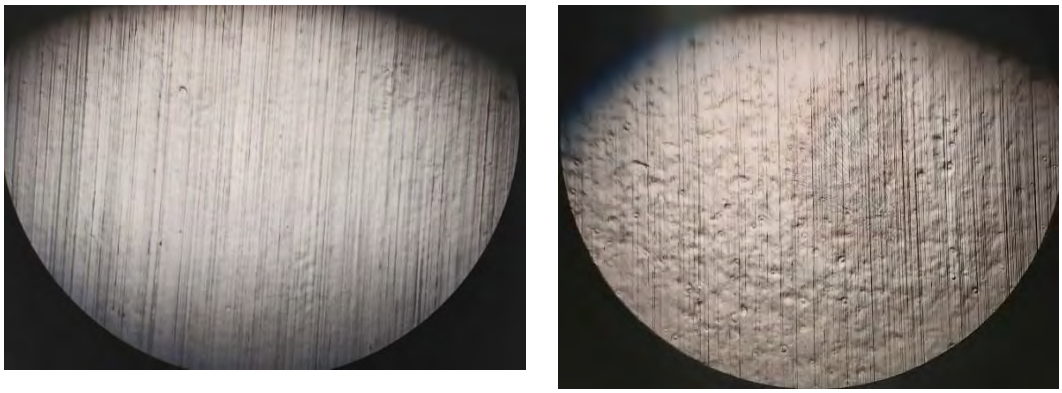

Figure 14: Cathode before (left) and after polishing in test (P3S5-3) (right). Both images are 40x zoom.

Through preliminary tests it can be concluded that electropolishing is indeed removing metal mass and improving the reflectivity of the cathode using the conditions outlined by ASTM B912. To better understand the optimal current density and potential, further tests are required.

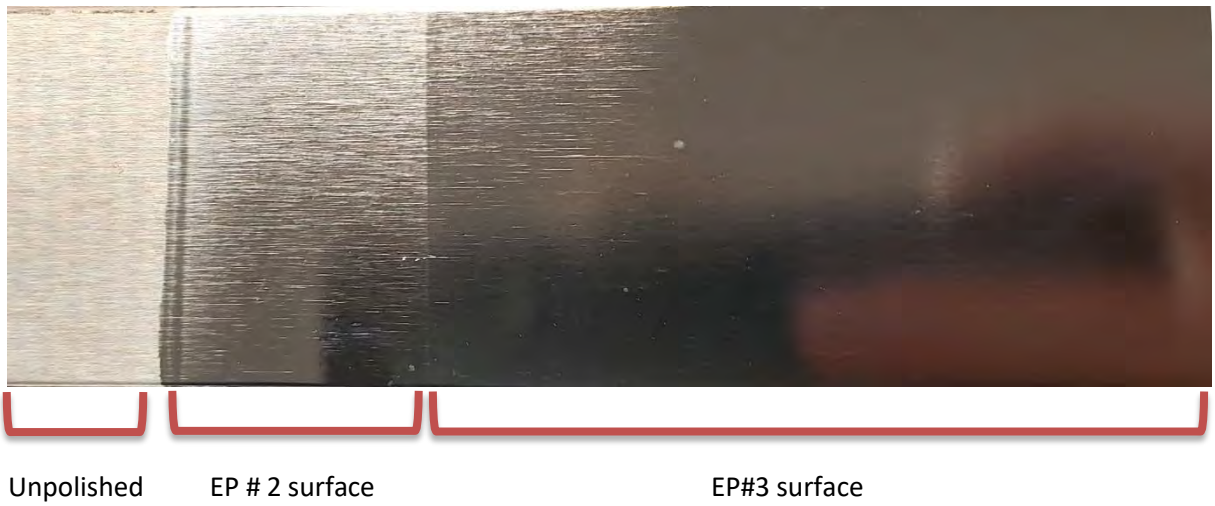

Figure 15: Comparison of electropolishing experiment 2 and 3 performed on a brushed 316 stainless steel electrode.

4.1.7 Electropolishing using formula used in China electrolyte

E25 asked MPI to evaluate and focus the project on the electropolishing method used in the Chinese EMM industry. The information given in the Chinese memos states the Chinese EMM plants use 304 stainless steel for cathodes. After contacting many local suppliers, and enlisting a local machining shop, no suppliers stocking regular 304 were found. The list of suppliers contacted is found in Table 8. Most stated on their website they sell 304, however when material certifications were requested, the carbon content was always to the low carbon quantity of < 0.03% carbon. One of the suppliers the local machine shop contacted said they don't think anyone in WA will sell 304 stainless steel that is not low carbon.

Table 8: Suppliers contacted

Supplier Contacted
Bohler
Action Laser Cutting
Stirlings Performance Steels
CoolSteel
Midway Metals
Voestalpine
Vulcan Stainless

On further investigation, most of the 304 supplied is "dual-grade," or "dual-certified" This means the composition (see Table 9) and mechanical properties conform to both the 304 and 304L. The mechanical specifications differ depending upon the dimensions of the steel, however 304 generally has a higher minimum tensile strength and yield strength requirement due to the higher carbon content.

Table 9: Comparison of 304 stainless steel composition

	C	Mn	P	S	Si	Cr	Ni	N
304	0.08	2.00	0.045	0.03	0.75	18-20	8-10.5	0.1
304L	0.03	2.00	0.045	0.03	0.75	18-20	8-10.5	0.1
304H	0.04-0.1	2.00	0.045	0.03	0.75	18-20	8-10.5	

There appears to be two reasons why 304 stainless steel is not commonly sold;

1. Cheaper for a steel manufacturer to produce one type of stainless steel than two (304 + 304L vs dual certified)

2. Lower carbon content reduces chromium carbide precipitation in welding, which can cause corrosion at the welds due to removal of chromium from the steel.

After searching for 304 with standard carbon 0.03% < C% ≤ 0.08%, steel strips of dual certified 304/304L were purchased for lab scale tests.

4.1.8 Linear sweep voltammetry

Figure 16 shows the anodic curves obtained a linear sweep voltammetry scan the electrolyte with the formula used in China supplied by E25 (3 parts by weight H_3PO_4, 2 parts H_2SO_4 and 0.1 parts glucose) at 60 ± 2 °C. The test was carried out in a three electrode system with use of Pine Wavenow potentiostat/galvanostat.

The tested electrode was 304/304L dual grade stainless, reference electrode – Ag/AgCl electrode and the counter electrode was a 316 stainless steel electrode. From Figure 16, the plateau occurred in the potential range: 1.58 – 1.83 V (Ag/AgCl) and the corresponding current densities from 0.18 – 0.19 A/m^2.

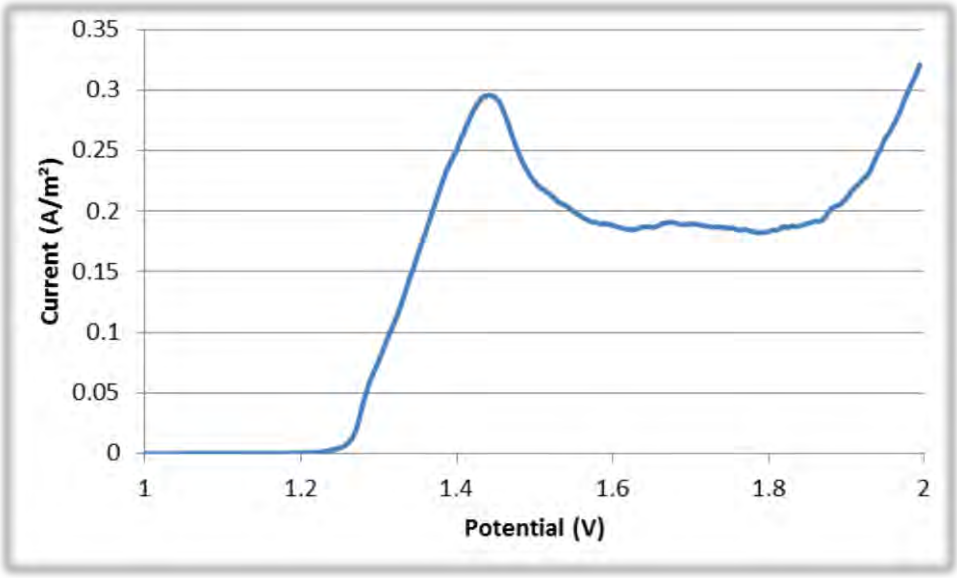

Figure 16: Linear sweep scan of electropolishing solution formula used in China using a 304/304L dual grade stainless steel anode and 316 stainless steel cathode. The scan rate was 1 mV/s.

a. Electropolishing preliminary test (P3S5-4)

The first electropolishing test on 304/304L stainless steel strips was conducted under the same parameters used in China (Communication between Neil Graham and Aleks Nikoloski). These are summarised in Table 10. The purpose of this test was to observe the surface finish after using a current density within the range disclosed by China (350-400 A/m^2). The apparent current density tested was 400 A/m^2. Remarkably, the potential was ~2.92V which is much lower than the value observed by China (5 – 7 V). This low potential value may be related to type of the cathode used in our test which was a 316 stainless steel. Lochynski et al [16] used stainless steel plate as anode and cathode with same size.

Knowing the type of cathode used in China will be beneficial for our test.

Table 10: Electropolishing test parameters for P3S5-4.

Variable	Value
Anode	New 304 stainless steel strip with 2B finish
Cathode	316 stainless steel
Electrolyte composition	Chinese electrolyte (3 parts H_3PO_4, 2 parts H_2SO_4 0.1 part glucose)
Time	10 minutes
Temperature (ºC)	58 ºC
Apparent current density	390 A/m^2
Potential	~2.92 V
Electrode gap	8 cm

Images of the electrode after 10 minutes of polishing can be seen in Figure 17. It appears the apparent current density was not high enough in all areas of the electrode to achieve polishing. The apparent current density is

higher at the edges due to the edge effect, which is a possible reason why the edges are more visibly polished than the middle.

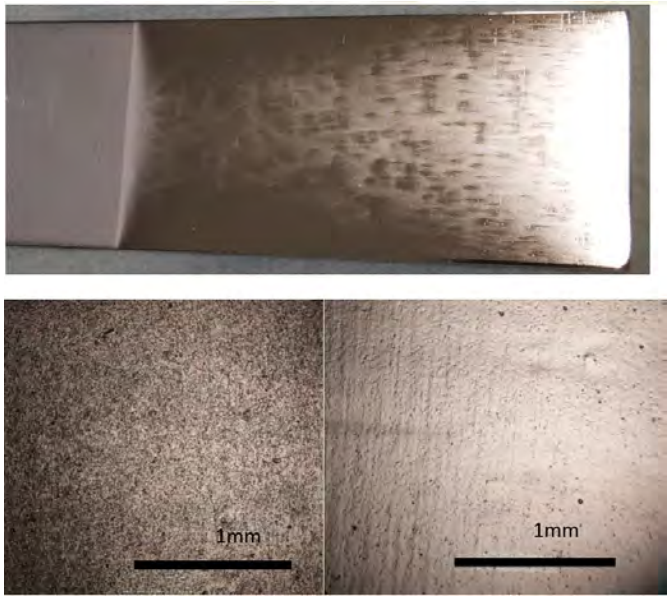

Figure 17: Photo of 304 after polishing at 400 A/m^2 (top) and images under the microscope of the inner dull areas (bottom left) and outer more polished sections (bottom right).

b. Electropolishing preliminary test (P3S5-5)

In this test, the potential was set to 7V (China use 5V – 7V) instead of setting the apparent current density. This resulted in an apparent current density of 1660 A/m^2, much greater than previously tested. The variables of the test are demonstrated in Table 11.

Table 11: Electropolishing test parameters for P3S5-5

Variable	Value
Anode	New 304 stainless steel strip with 2B finish
Cathode	316 stainless steel
Electrolyte composition	Chinese electrolyte (3 parts H_3PO_4, 2 parts H_2SO_4 0.1 part glucose)
Time	10 minutes
Temperature (ºC)	59 ºC
Apparent current density	~ 1660 A/m^2
Potential	~ 7.0 V
Electrode gap	8 cm

The resulting finish appears more even and uniform (Figure 18) than the previous test at 400 A/m^2, however there are some vertical marks or lines running the length of the polished area. They aren't pitted holes as seen in previous polishing tests that used 316 stainless. It is possible this is may be due to a similar mechanism although it is not yet certain the cause of these marks.

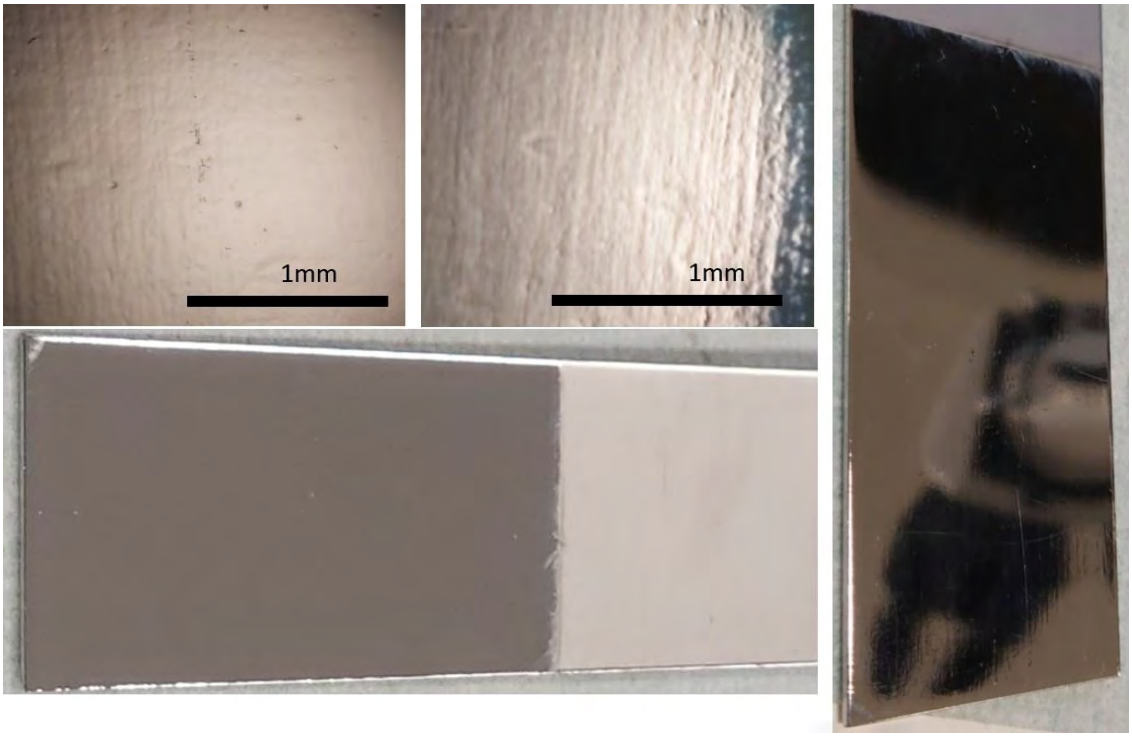

Figure 18: Microscope images of regular and low light (top left and middle), and images of the polished electrode (bottom and right)

c. Electropolishing preliminary test (P3S5-6)

The potential was lowered to 5V in this test, the lower limit of what the Chinese are reported operating at. The resulting apparent current density was 1050 A/m^2.

Table 12: Electropolishing test parameters for P3S5-6

Variable	Value
Anode	New 304 stainless steel strip with 2B finish
Cathode	316 stainless steel
Electrolyte composition	Chinese electrolyte (3 parts H_3PO_4, 2 parts H_2SO_4 0.1 part glucose)
Time	10 minutes
Temperature (ºC)	59 ºC
Apparent current density	1050 A/m^2
Potential	~5 V
Electrode gap	8 cm

The resulting polished finish was examined under microscope and is visible in Figure 19 below. There is very obvious pitting present, showing a worse surface finish than the higher 7 V test.

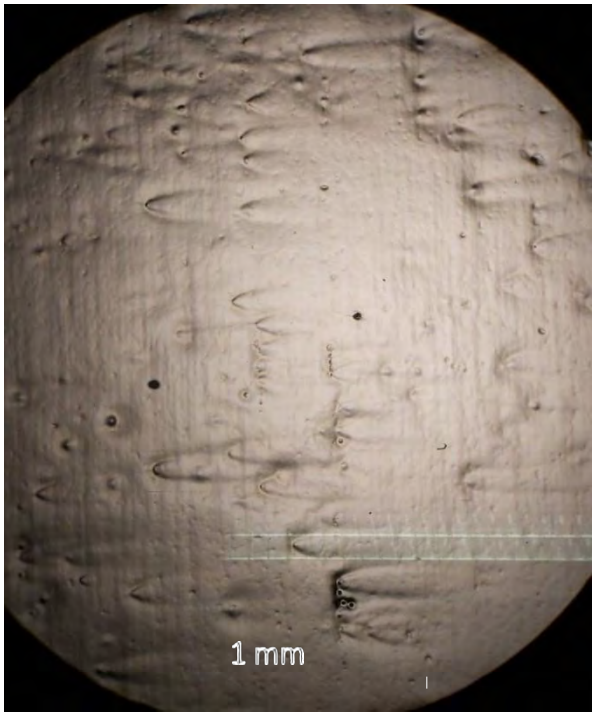

Figure 19: Stainless steel polished using Chinese electrolyte and 5V.

4.2 Electrowinning Tests

Two electrowinning tests were conducted, both using brand new 304 cathodes with a 2B finish. The first test was a 4-hour test using lower concentration manganese electrolyte (15g/L) than used in Phase 1 and 2 and the second was a 24-hour test using the same parameters as the 4-hour test.

4.2.1 4-hour test

The purpose of this test was to compare the deposit against the 4-hour deposit formed on a 316 stainless steel cathode and note if any differences were observed. Throughout the experiment, the voltage, current, and catholyte pH were recorded. Anolyte pH recording was unable to be performed during this experiment however following this test the pH setup was altered in order to record the anolyte pH in future tests. The recorded data is displayed in Figure 20 and Figure 21. Note that Figure 20 shows a current density of ~330 A/m^2. The actual current was measured using a multimeter, which gave a slightly different, more accurate representation of the current passing through the cell. The multimeter was kept at a reading of 1.321 A, giving a current density of 320 A/m^2 at the cathode. The potential began at ~5.2 V upon commencement of the experiment but within two minutes, it dropped to ~4.6 V. The potential continued to fall throughout the duration of the test, ending up at ~4.4 V after 4 hours.

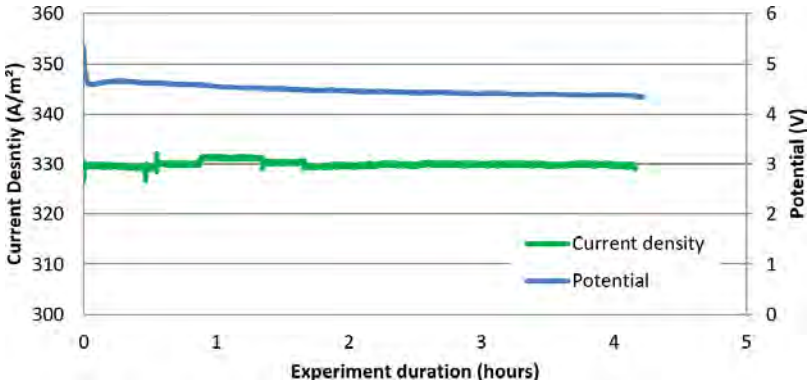

Figure 20: Current density and potential readings for the 4-hour manganese electrowinning test.

The pH of the catholyte is shown in Figure 21, and remains slightly basic, increasing from a pH of 7 to 7.3 after 4 hours.

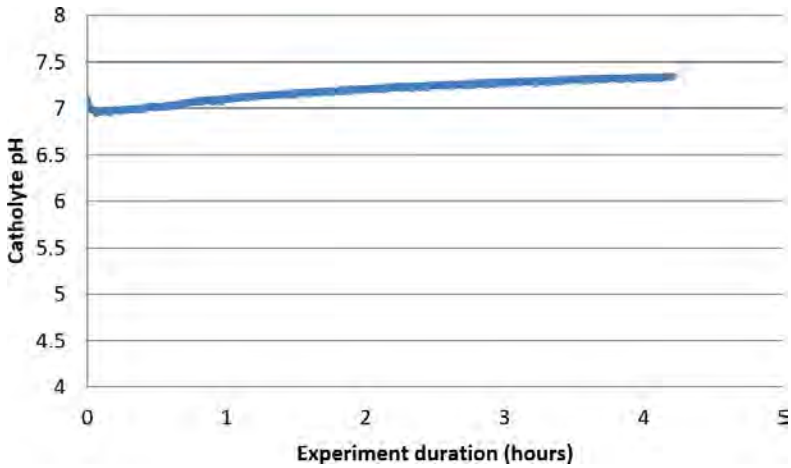

Figure 21: Catholyte pH over the 4-hour test

The resulting deposit is shown in Figure 22, and weighed 4.819 g, resulting in a current efficiency of 84% and energy consumption of 5.086 kWh/kg. Note these results are similar to a previous test conducted using 15 g/L Mn and a 316 stainless steel cathode with a current density of 320 A/m^2 (82% and 5.342 kWh/kg). Higher current efficiencies (>92%) were observed in phase 2 of the project; however those tests were operating at a much higher manganese concentration of 48 g/L.

Figure 22: Manganese deposit on 304 stainless steel cathode after 4-hour of electrowinning.

After the test had concluded, volumes were measured, and samples were taken to perform a selenium mass balance. The results are yet to be received however they will be presented within the next interim report.

4.2.2 24-hour test

Following promising results from the 4-hour test using 304 stainless steel cathodes, a 24-hour test was performed under the same conditions (15 g/L Mn, 320 A/m^2). The current density and cell potential as well as the catholyte and anolyte pH are shown in Figure 23 and Figure 24 respectively. During the start of the experiment, there was some current fluctuation, possibly due to a faulty connection. This fluctuation was greatly reduced after the first hour, after which the current remained quite steady for the remainder of the experiment. The potential had reduced to ~4.3 V after 24 hours of operation.

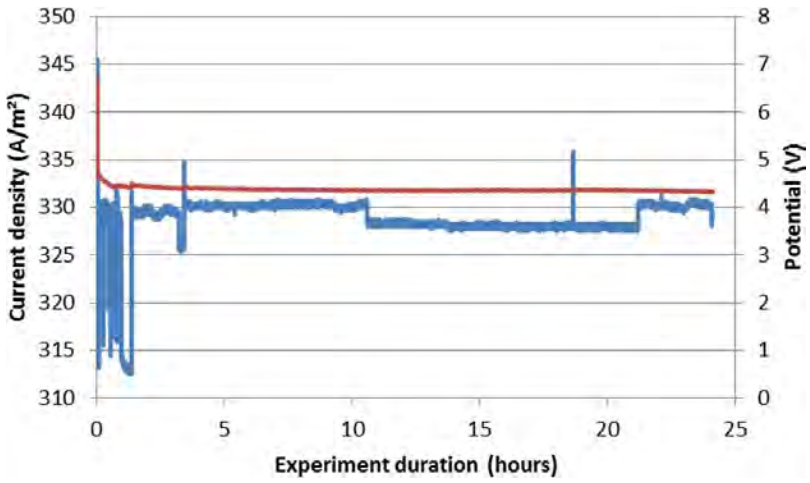

Figure 23: Current density and cell potential over the duration of the 24-hour manganese EW test.

The pH of the catholyte reached 7.8 after 24 hours, increasing from 7.0 at the start of the test. No addition of acid was used to control the pH. The pH of the anolyte dropped to 1.4.

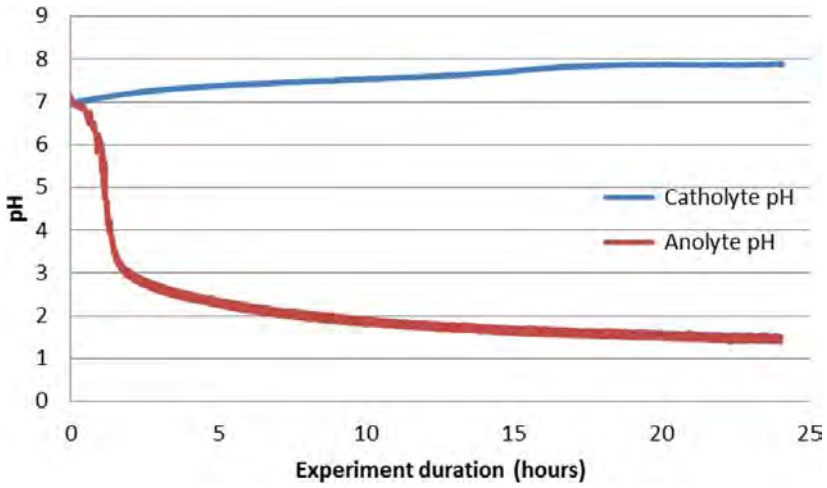

Figure 24: Anolyte and catholyte pH over the 24-hour manganese EW test.

The resulting deposit weighed 14.17g, giving a current efficiency of 43% and energy consumption of 9.89 kWh/kg. It is shown in Figure 25.

Surprisingly, the Mn deposit contains black area, still to be analysed, and very shiny and smooth EMM. The presence of the black region needs further investigation. A full analysis for both areas will be conducted, and the results will be conveyed in the next interim report.

Figure 25: Manganese deposit from the 24-hour test.

4.2.3 Deportment of selenium in 4-hour test

Selenium is commonly added to manganese sulfate electrolyte to enhance the current efficiency of the electrowinning process where Electrolytic Manganese Metal (EMM) is produced. The elemental selenium is concurrently reduced with manganese on the cathode. The percentage of selenium in the produced EMM, generated in phase 1 and 2, ranges between 0.1 and 0.2 % of the produced metal, this represents only 3% of Se from feed. A considerable amount of the remaining selenium left in the system ie electrolyte and precipitate.

The deportment of selenium during 4-hour electrowinning test stated in Section 4.2.1 was done by taking samples from each part of the electrowinning cell like feed, catholyte, anolyte…etc and the total volume of each part of the system was recorded.

The electrolyte feed consists of approximately 25 ppm selenium. The samples from the 4-hour test and three control samples were sent to three independent laboratories. The labs were Marine and Freshwater Research Laboratory (MAFRL), Nagrom and Murdoch University. The ICP-MS results from all three labs appear to be consistent. Results from control samples suggest that ICP-MS results from MAFRL is the most precise, followed by Nagrom and Murdoch. Results are summarised in Table 13,Table 16 Table 18.

The possible deportment of selenium (Se) will be:

73% Se in the system was accounted for from the analysis, the difference of 27% Se could be found in the anode sludge or precipitate from catholyte and anolyte sludge. Both anolyte sludge and precipitate from catholyte were not assayed due to the insignificant amount recovered. The majority of anolyte sludge and/or precipitate from catholyte consist of manganese dioxide. It is well known from literature that Selenite (Se(IV) may adsorb on manganese dioxide. Balistrieri and Chao [17] investigated selenium adsorption on iron and manganese dioxide, the authors concluded that even Se adsorption on amorphous iron oxyhydroxide is stronger than manganese dioxide, Se(IV) adsorption on manganese dioxide increases with decreasing pH. Selenate (Se(VI)) does not adsorb on manganese dioxide.

Two catholyte samples were submitted for Se analysis. One sample had a pH 7 and the other was acidified before submission. There was a 30% difference in Se concentration between the two samples. The Se concentration in the acidified catholyte sample was higher.

The majority of the Se was not found in the EMM deposit (only 3% Se from feed or 14% Se from catholyte solution). Se composition in metal was 0.13% which is consistent with the previous 4-hour tests.

In order to confirm the adsorption of Se on MnO_2, it is recommended to:

- Filtered anode sludge and precipitate from catholyte that were "stuck" to the filter paper to be dissolved in acid with the intention to dissolve any Se in them for assay.
- Recommended another test but for 24 hours to produce more anode sludge and precipitate from catholyte for assay.

Cobalt and Nickel analysis show that the concentration of both elements increase during the test. This observation needs more study to understand the mechanism of this increase.

Table 13: Electrolyte analysis performed at **MARINE (78SE)**

		Co	Ni	Se	Co	Ni	Se	
	Volume (L)	mg/L	mg/L	mg/L	mg	mg	mg	
Feed	7.52	0.3	0.20	27	2.25	1.50	202.90	100%
Cath Cell	1.45	1.2	0.24	16	1.74	0.35	23.20	11%
Cath Bleed	1.09	1.3	0.27	20	1.42	0.29	21.80	11%
Anol Cell	3.87	1.2	0.43	22	4.64	1.66	85.14	42%
Anol Bleed	0.55	0.44	0.36	23	0.24	0.20	12.65	6%
				Se				
	Mass (kg)	mg/Kg	mg/Kg	mg/Kg	mg	mg	mg	
Mn Metal	0.0048193	260	70	1300	1.25	0.34	6.26	3%
		0.026%	0.007%	0.130%				

Table 14: Accountability from MARINE

Accountability (Co) %	412%
Accountability (Ni) %	189%
Accountability (Se) %	73%
Accountability (Volume) %	93%

Table 15: Mass percentages MARINE

Co in feed (mg)	2.2545
Co in EMM (mg)	1.2530
% total Co in EMM	56%
Ni in feed (mg)	1.503
Ni in EMM (mg)	0.3374
% total Ni in EMM	22%
Se in feed (mg)	202.905
Se in EMM (mg)	6.2651
% total Se in EMM	3%

Table 16 Selenium NAGROM 82SE

		Co	**Ni**	**Se**	**Co**	**Ni**	**Se**	
	Volume (L)	mg/L	mg/L	mg/L	mg	mg	mg	
Feed	7.515	<1	<1	25			187.875	100%
Cath Cell	1.45	1	<1	16	1.45		23.2	12%
Cath Bleed	1.09	1	<1	18	1.09		19.62	10%
Anol Cell	3.87	1	<1	21	3.87		81.27	43%
Anol Bleed	0.55	<1	<1	22			12.1	6%
				Se				
	Mass (kg)	mg/Kg	mg/Kg	mg/Kg	mg	mg	mg	
Mn Metal	0.0002833	240	85	35	1.156632	0.4096405	0.0099155	0%
		0.024%	0.009%	0.004%				

Table 17 Accountability from NAGROM

Accountability (Se) %	72%
Accountability (Volume) %	93%

Table 18 Selenium MURDOCH 80 SE

		Se	**Se**	
	Volume (L)	mg/L	mg	
Feed	7.515	21	157.815	100%
Cath Cell	1.45	14	20.3	13%
Cath Bleed	1.09	16	17.44	11%
Anol Cell	3.87	18	69.66	44%
Anol Bleed	0.55	20	11	7%
		Se		

Table 19 Accountability from Murdoch

Accountability (Se) %	75%
Accountability (Volume) %	93%

4.2.4 SEM-EDX report of unknown black substance

The EMM deposit from the 24-hour electrowinning test was noticeably black around its edges especially the region nearest to the solution line (see Figure 26). Careful inspection shows that the black regions were thinner than the metallic region at the centre of the EMM deposit. Also, worth mentioning is that nodules were not formed on one side of the edge taped with electroplating tape, whereas it was typical to find nodules growing around the edges taped with electroplating tape.

Figure 26. Black regions seen on edges of EMM deposit from 24-hour electrowinning test

Further "post-mortem" of the EMM deposit shows that the black regions were actually metallic in substance, possibly manganese metal, coated with an unknown black powdery compound. This is likewise the case with the electroplating tape that appears to be "burnt" whereby in actual fact the tape was undamaged but only coated with the unknown black powdery compound.

It was therefore of great interest to identify the black powdery compound.

The black powdery compound was recovered from the deposit as much as practically possible for characterisation by XRD, SEM and EDX. However, the small amount of black powdery compound that can be recovered makes it impossible for XRD analysis. Hence, only the SEM and EDX analyses were conducted on the black powdery compound as well as a metal piece with a black region intact (see Figure 27).

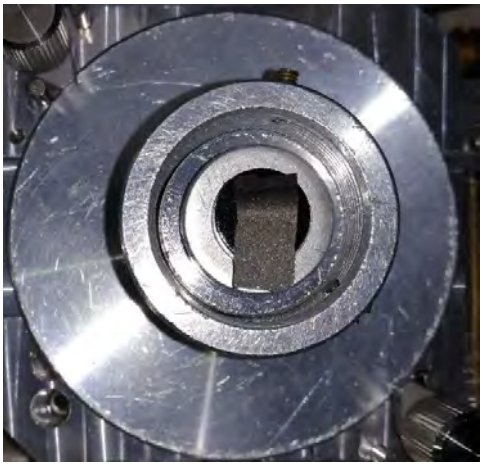

Figure 27. Metal piece placed on SEM stub using a carbon tape before mounted on SEM instrument

The unknown black powdery compound was mixed with ethanol and the created slurry was smeared on top of a carbon tape placed on a SEM stub before mounted on the SEM instrument. Figure 28 shows the SEM backscattered imaging and the EDX spectra of the unknown black powdery compound. The EDX spectra in Figure 28 were adjusted and normalised to the highest peak.

It can be seen that the powdery compound is in tens of micron size or less. Backscattered imaging also allows one to obtain compositional data of the sample area being analysed. In this instance, the backscattered image in Figure 28 suggests that the powdery compound is made of a uniform substance. This is consistent with its EDX area scan which identified the substance in the sample area as predominantly manganese. Other elements detected were chromium, cobalt, copper, oxygen, selenium, sodium, sulphur and zinc. EDX spot analyses confirmed that

manganese was consistently detected in the different spots across the sample area except for Spot 10 but other elements were only detected occasionally.

Chromium was introduced onto the sample surface from the passivation treatment of the EMM deposit. Cobalt, selenium, sodium, sulphur and zinc would have originated from the feed solution. On the other hand, copper was not part of the feed solution composition but the fact that it was only detected once suggest that this might be an error. The detection level of oxygen was quite high in certain spots, i.e., Spot 01, 02, 06, 09, 12 and 14. Given the low detection level of sulphur in those spots, it is unlikely that manganese sulphate in the feed solution precipitated on the sample surface, but this could be an indication of the presence of some sort of oxides, possibly of manganese.

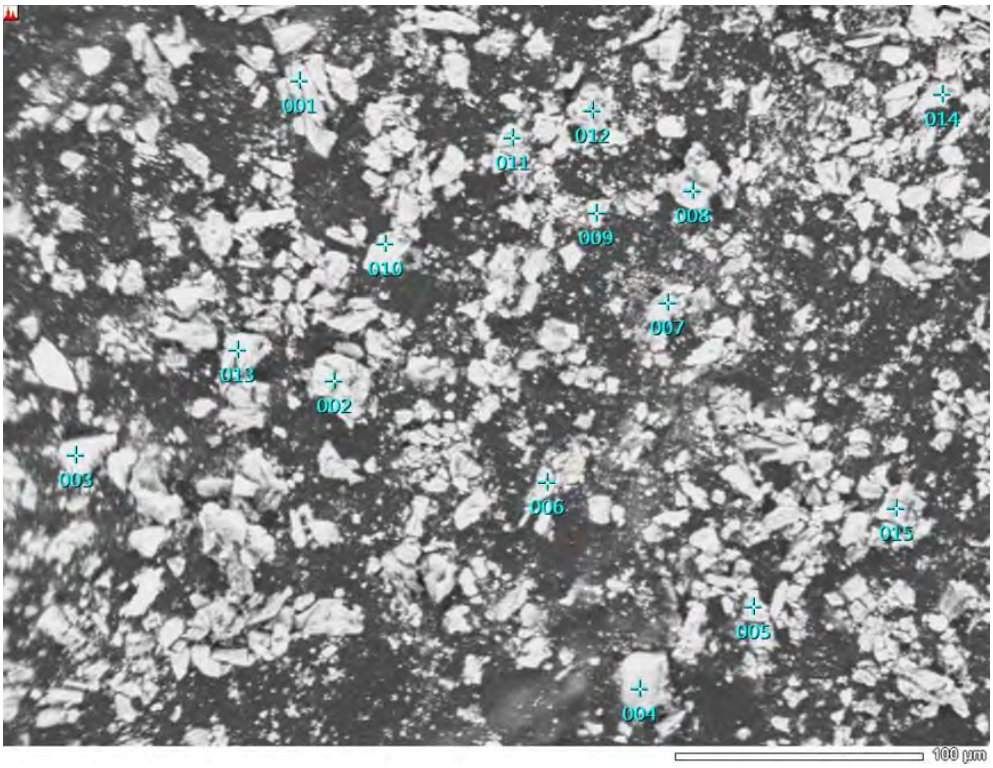

Figure 28. Normalised EDX spectra of spot analyses and area scan of unknown black powdery compound

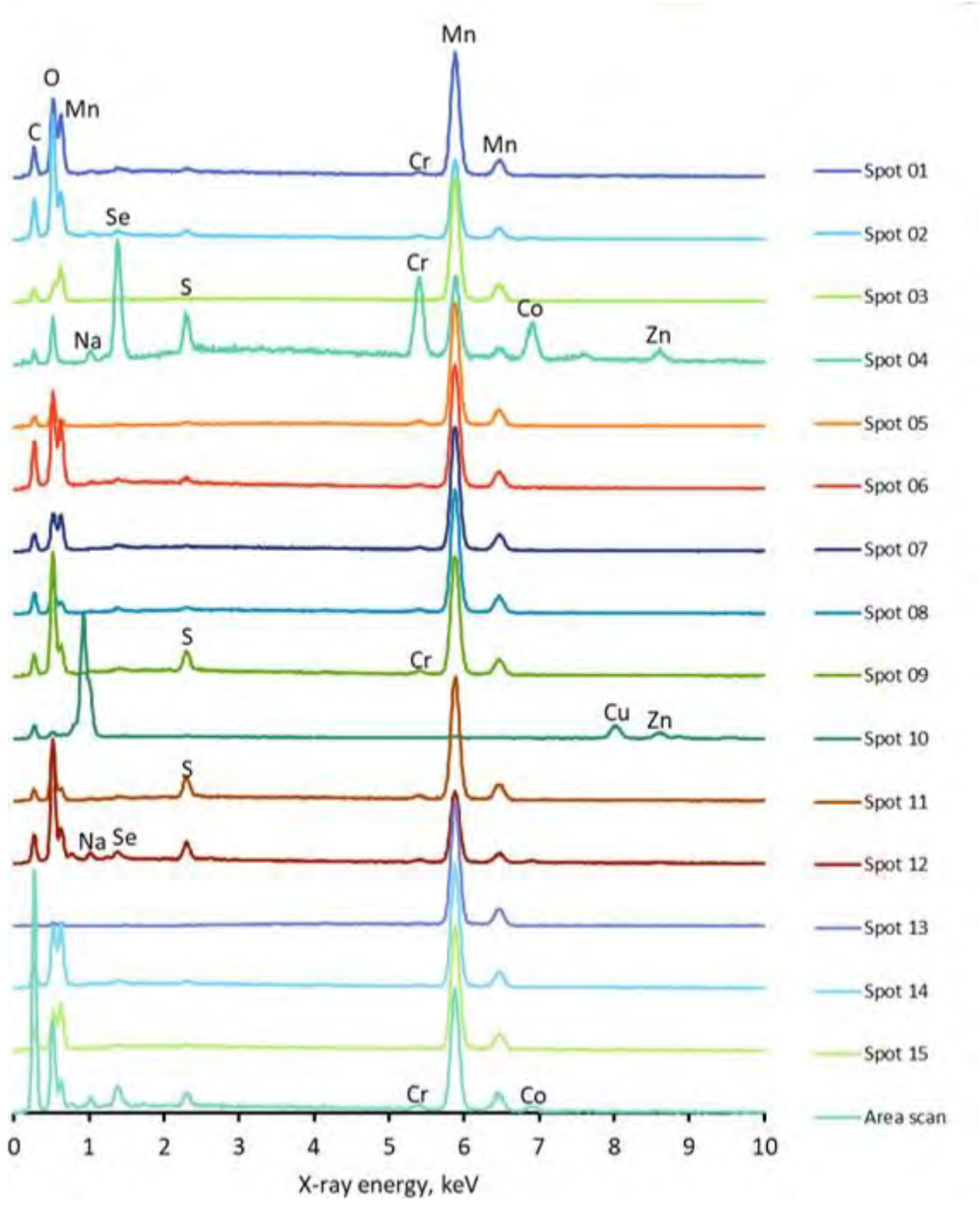

Figure 28. Normalised EDX spectra of spot analyses and area scan of unknown black powdery compound (continued)

Figure 29 shows the SEM backscattered imaging of the metallic region of the metal piece. The backscattered image suggests that the sample area is made of a uniform substance. This is consistent with the EDX area scan which identified the substance in the sample area as purely manganese metal (see Figure 30).

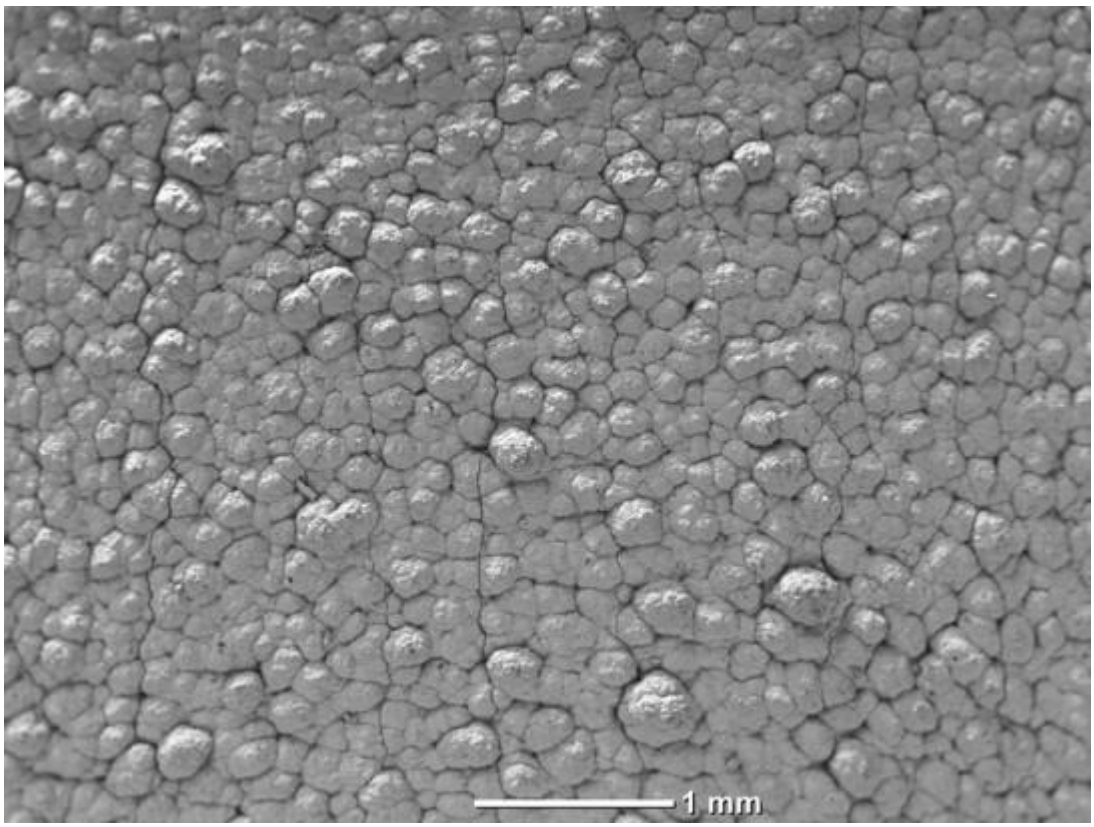

Figure 29. Metallic region of metal piece under SEM backscattered imaging

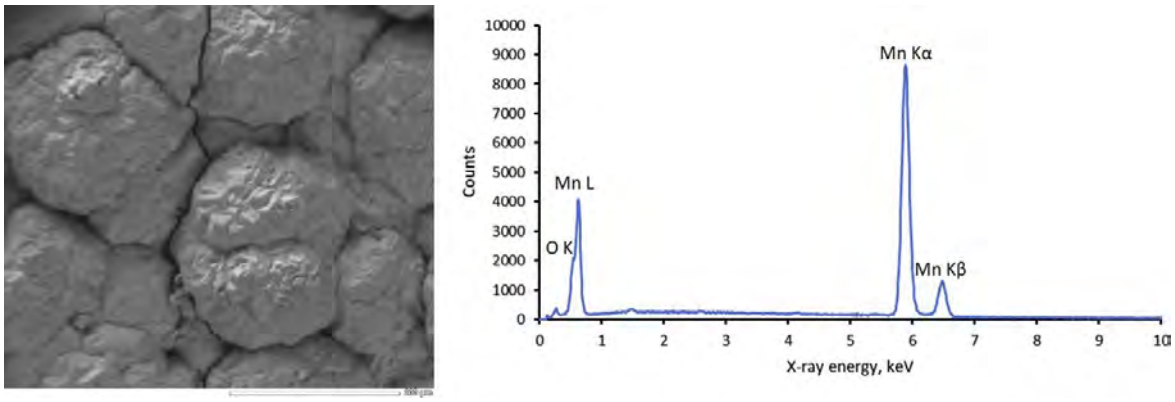

Figure 30. EDX area scan of metallic region of metal piece

In terms of the morphological structure of the metal piece, it resembles that of a typical EMM deposit plated on a stainless steel cathode surface (see Figure 31).

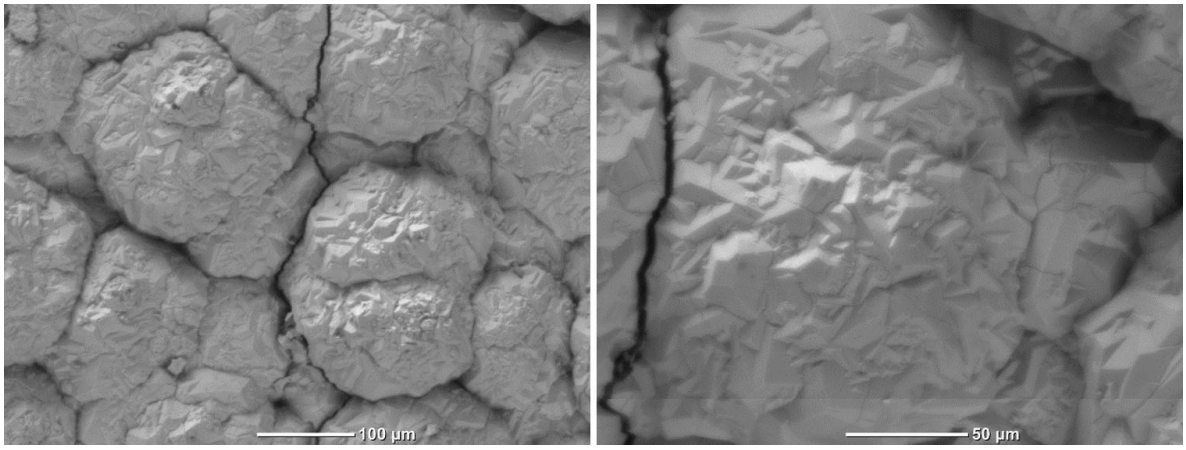

Figure 31. Morphological structure of metal piece

Figure 32 shows the black region of the metal piece under SEM backscattered imaging. The backscattered imaging of the sample area appears to suggest that the bright area (bottom of Figure 32) is similar to the metallic region of the sample. The darker area (middle of **Figure** 32) implies a different make-up from the metallic region of the sample, whereas the darkest area (top of Figure 32) is the carbon tape used to attach the metal piece to the SEM stub.

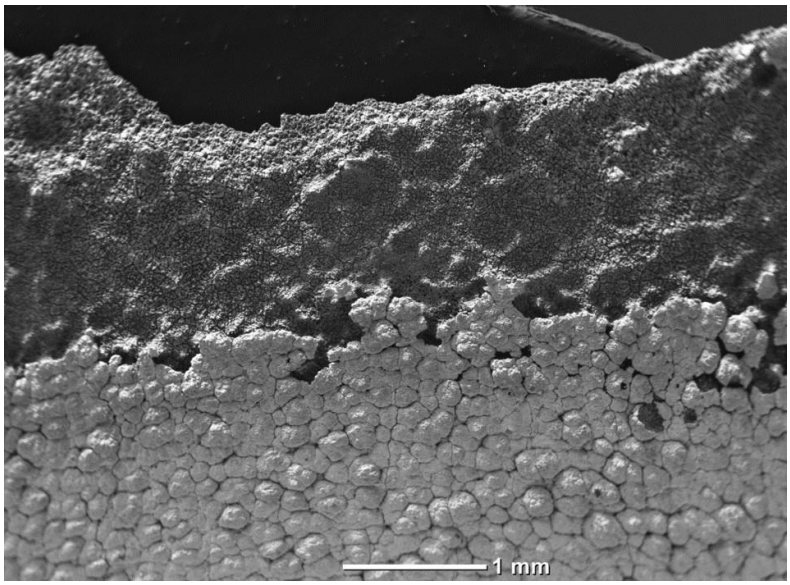

Figure 32. Black region of metal piece under SEM backscattered imaging

EDX analysis was performed on the darker area (middle of Figure 32) in an attempt to identify its composition. The EDX spectra in Figure 33 shows that manganese and chromium were consistently detected with manganese being the predominant element. Most likely chromium was introduced onto the sample surface from the passivation treatment of the EMM deposit. Other elements, *i.e.*, calcium, oxygen, selenium and sulphur were occasionally detected but in trace amounts (except for oxygen) and may have originated from the feed solution. This elemental composition appears to be quite similar to that of the black powdery compound previously analysed. It was also observed that the detection level of oxygen was quite high in certain spots, *i.e.*, Spot 01, 03, 06, 07 and 09. Given the low detection level of sulphur in those spots, it is unlikely that manganese sulphate in the feed solution precipitated on the sample surface, but this could be an indication of the presence of some sort of oxides, possibly of manganese.

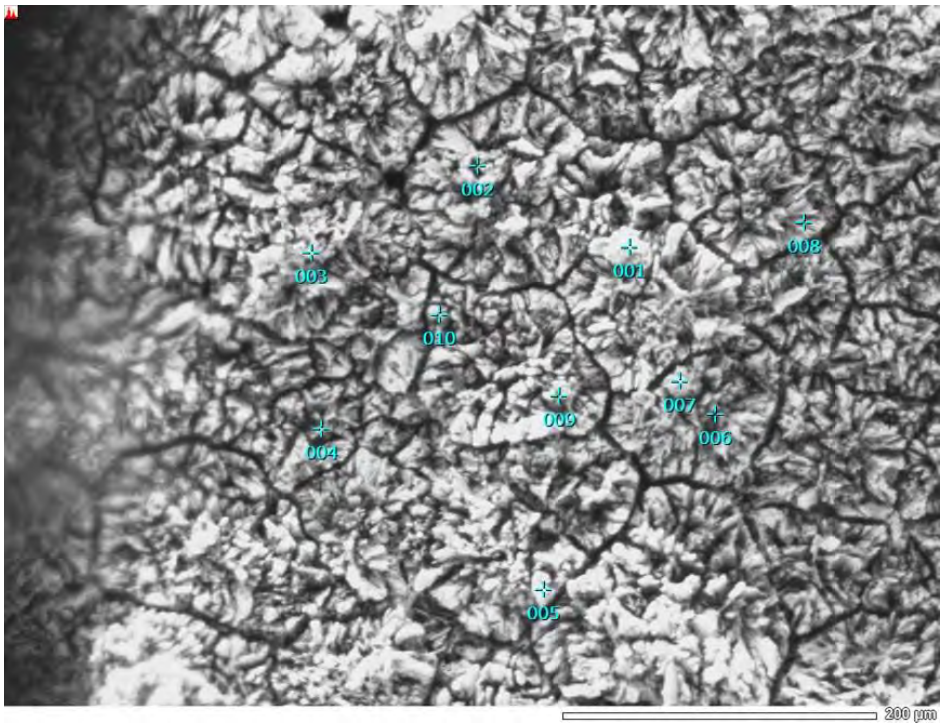

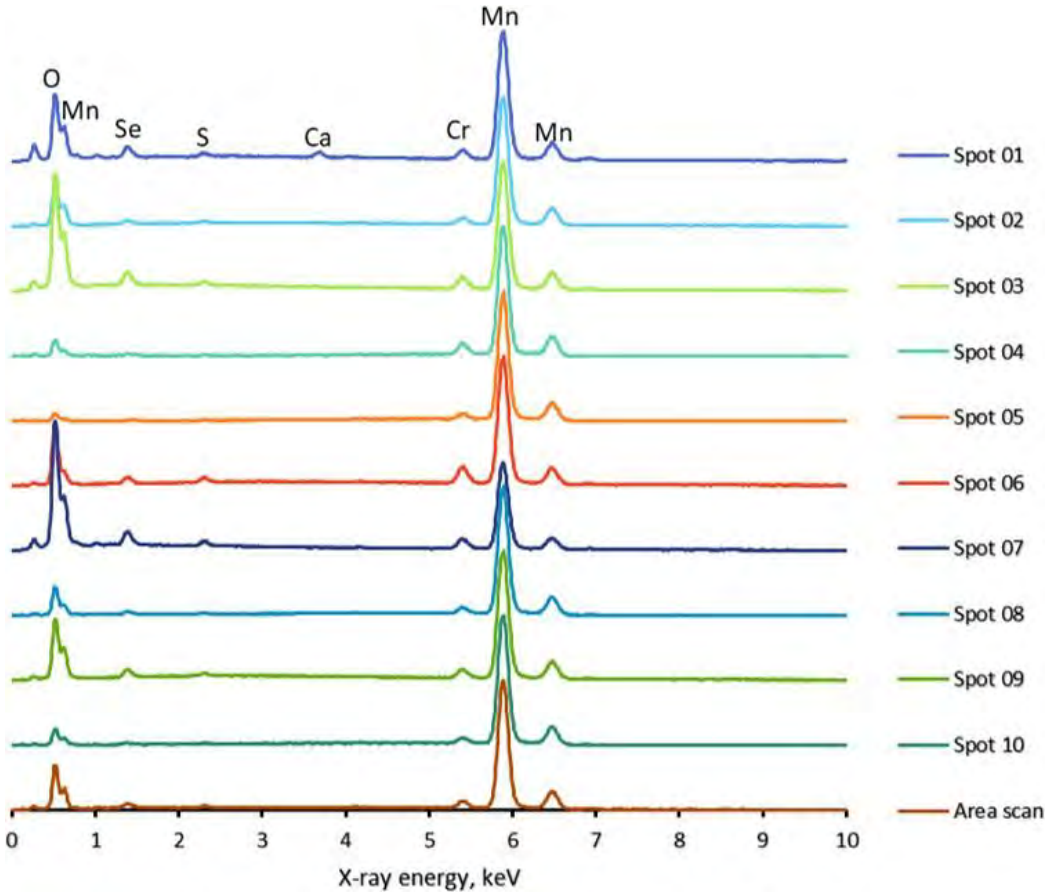

Figure 33. Normalised EDX spectra of spot analyses and area scan of the darker area (middle of Figure 32)

EDX spot analyses were performed on a different sample area showing both the bright area and the darker area. Figure 33 shows that there is but a vague difference between the two areas, *i.e.*, oxygen and sulphur was detected only in the darker area, whereas cobalt was detected only in the bright area. However, the detection of cobalt (and zinc) may be exaggerated from the normalised EDX spectra.

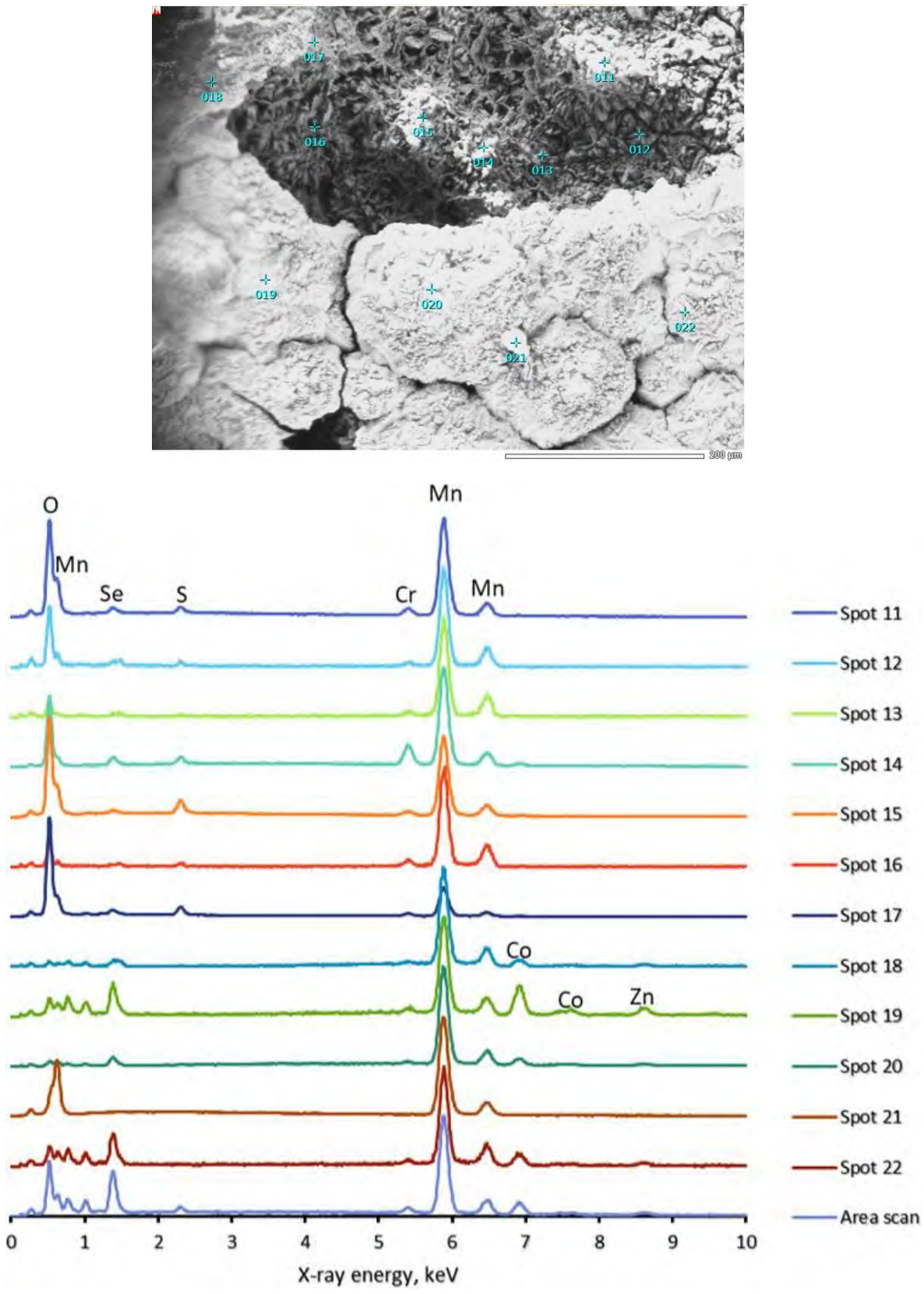

Figure 34. Normalised EDX spectra of spot analyses and area scan of black region of metal piece

4.3 Pilot Plant

This section of the report will summarise the dimensions of the EW cell and cathode and also the flow of electrolyte through the cell in its current state.

4.3.1 Current cell arrangement

The cell has inside dimensions of 770mm x 525mm x 660mm, as shown in Figure 35 below. This equates to approximately 250L at maximum capacity.

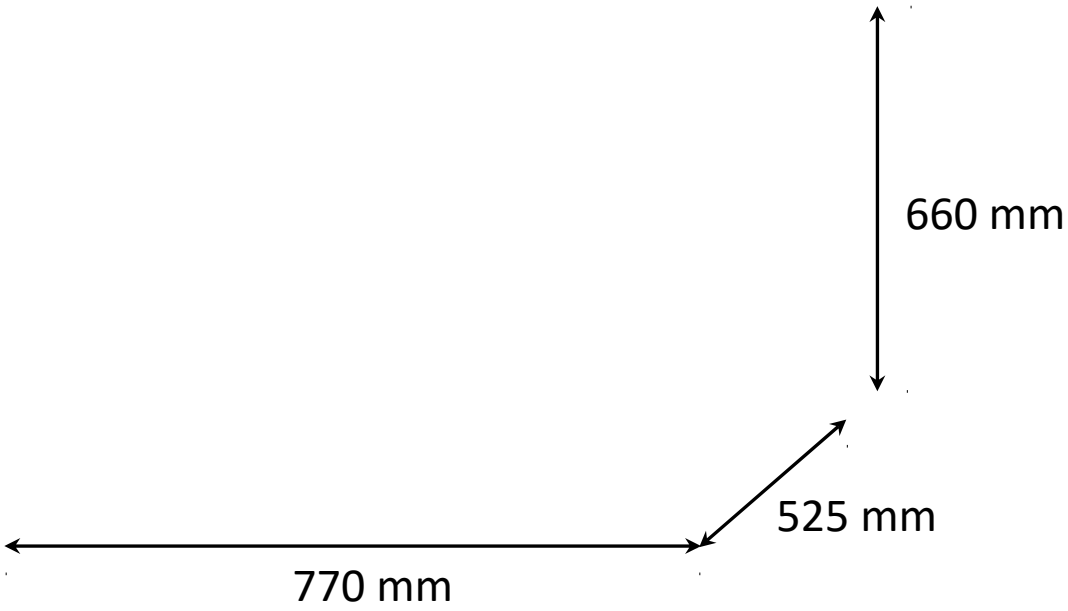

Figure 35: Current EW cell inside dimensions

The flow of electrolyte into and out of the cell is shown in Figure 36. There is an inlet (inside diameter 25mm) from the bottom of the tank, where the feed is introduced. This fills the cell, after which the electrolyte exits from an overflow weir. The height of the weir can be adjusted, allowing the electrolyte level in the cell to be adjusted and controlled. The inside diameter of the weir overflow pipe is 16mm.

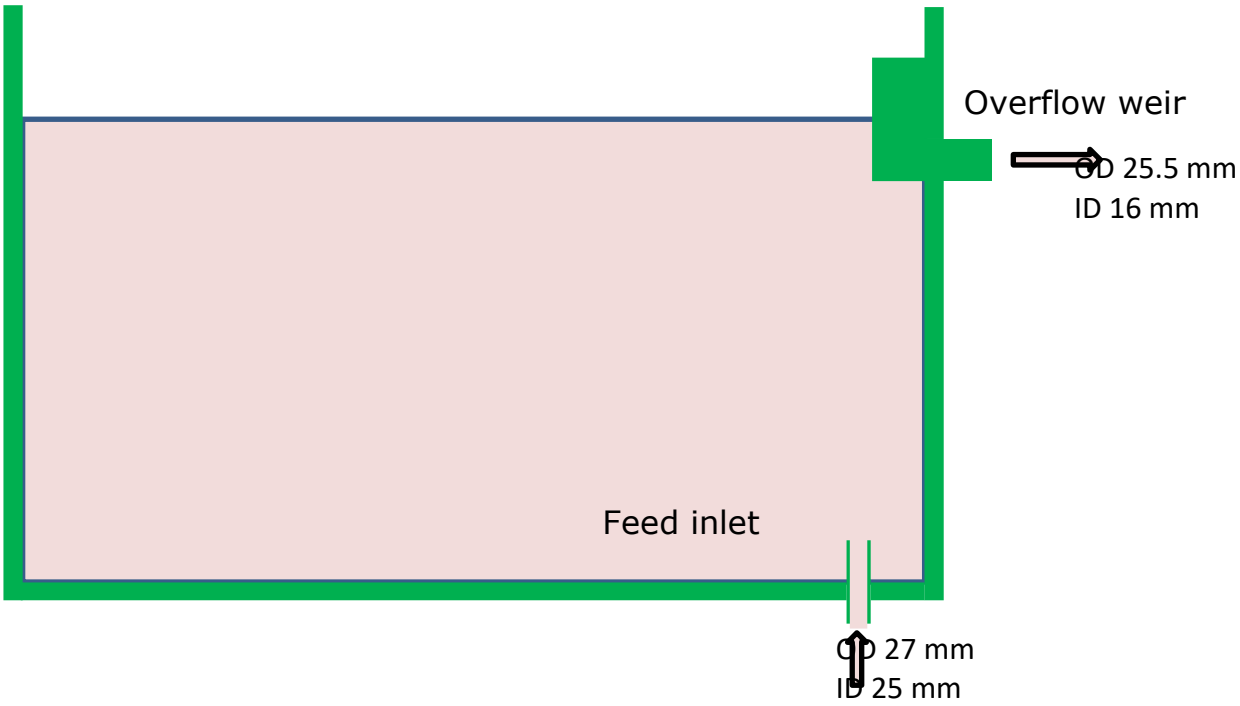

Figure 36: Side view of current EW cell showing feed inlet and overflow weir.

The dimensions of the cathodes originally used in this cell are shown in Figure 37. The busbar is 70cm wide, and from the bottom of the busbar to the bottom of the electrode is 60.5cm. Of the 60.5cm, only 46.5 cm is submerged in the electrolyte. The width of the cathode is 45cm, making the active area ~0.21m^2.

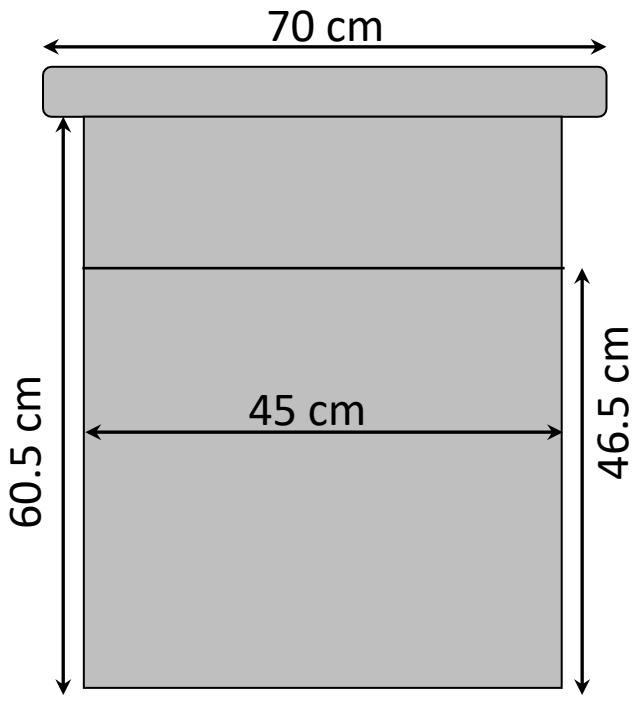

Figure 37: Current EW cell cathode dimensions

4.3.2 Proposed cell modifications

The pilot plant in its current state is not fit for manganese electrowinning. This is because there is no method of separation between the anolyte and catholyte, a strict requirement to ensure the manganese metal plated does not dissolve. To accomplish this separation, an additional, smaller PVC cell will be placed inside the pre-existing cell. The anodes (with diaphragm boxes) and cathodes will sit within this smaller cell. This is demonstrated in Figure 38. The smaller cell will sit 70mm from the bottom of the pre-existing cell, creating a false bottom. The purpose of this will become clear when the flow of electrolyte is discussed in the coming paragraphs.

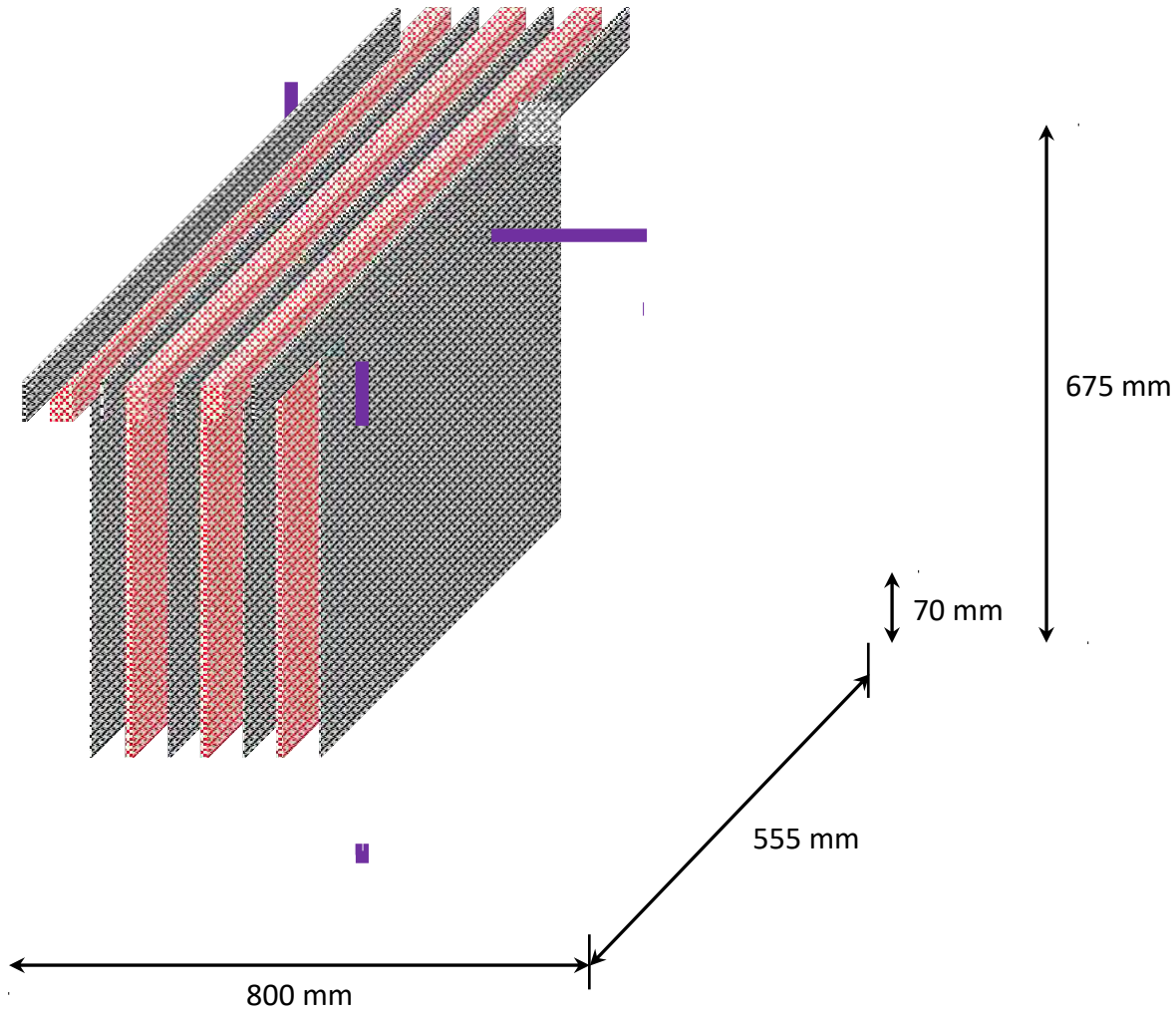

Figure 38: Outside dimensions of the pre-existing cell, showing the proposed smaller cell, which would be placed inside the larger cell. Note for simplicity the diaphragm boxes are not included in this diagram.

The proposed dimensions of the smaller cell are shown in Figure 39. The upper lip is to mimic the contour of the larger cell, a proven design for supporting electrodes.

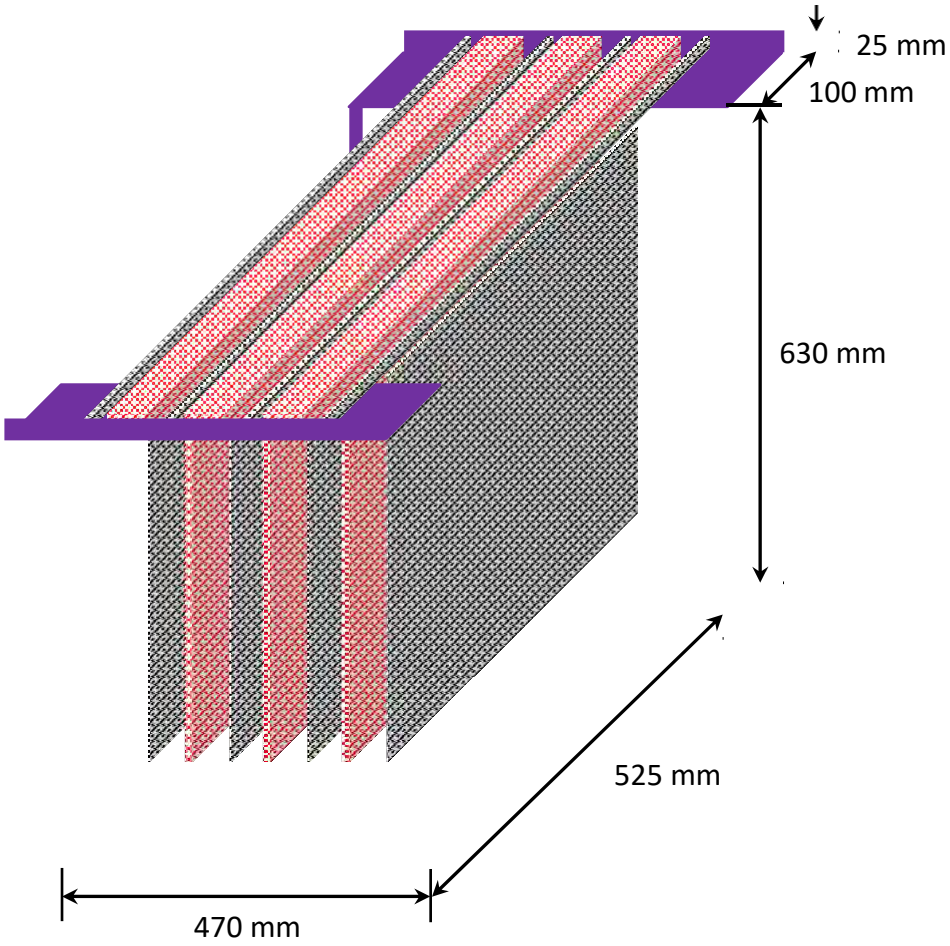

Figure 39: Proposed cell dimensions for the smaller cell, which will house the anodes and cathodes during operation.

The small cell will be constructed with a feed inlet at the bottom of the cell (inside diameter of 25mm), and an overflow that will direct catholyte back to the feed tank (inside diameter of 16mm). The distance from the bottom of the overflow outlet to the top of the cell is 55mm. The 70mm gap between the bottom of the small cell and large cell will be maintained by four feet. This is shown in Figure 40.

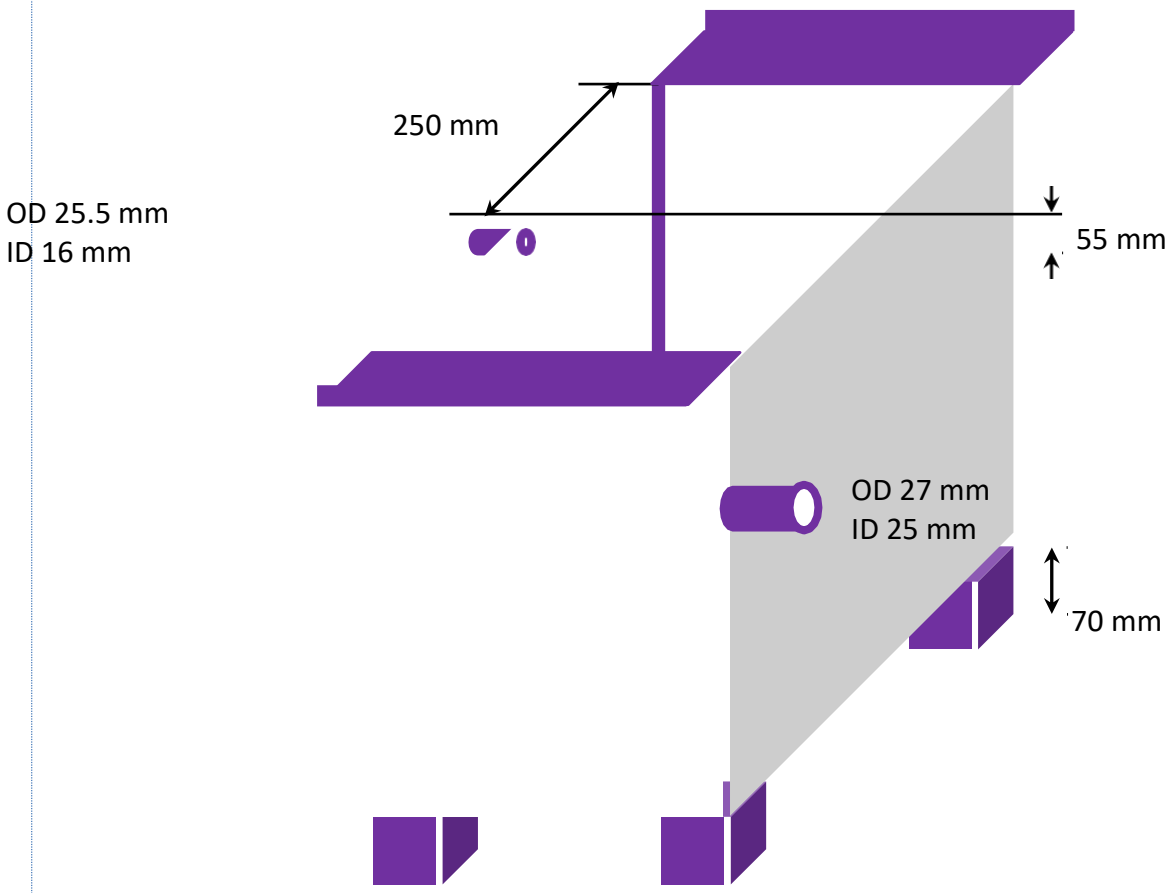

Figure 40: Inlet and outlet of small inner cell.

The flow of electrolyte and arrangement of cathode and anode will is shown in Figure 41. As described earlier, both the anodes and cathodes will sit within the small cell. To separate the anolyte and catholyte, the anodes will be placed in diaphragm boxes. These diaphragm boxes will connect to the larger cell via holes in the small cell. The exact method of attachment is yet to be decided upon, although a similar method to the bench scale setup may be possible, using a silicon pipe and male adapters on both the bottom of the diaphragm box and small cell.

The connection of diaphragm boxes to the large cell will facilitate the flow of anolyte from the cell to the pre-existing weir on the large cell. This allows for the anolyte level to be maintained. The cathodes will sit in the small cell, and all share the same catholyte solution, as opposed to being kept in boxes. The feed solution will be pumped from the feed inlet on the large cell into the feed inlet on the small cell. To assist in creating good quality deposits, feed solution will enter into the small cell underneath each cathode. This will be accomplished via a feed manifold, depicted by a green line on Figure 41.

A top view of this manifold is shown in Figure 42. The manifold will run directly underneath each cathode, replenishing the electrolyte through feed holes and assisting with mass transfer. Note in this figure the cathodes are absent in order to clearly see the manifold. In practice, they will be positioned directly above the manifold feed holes.

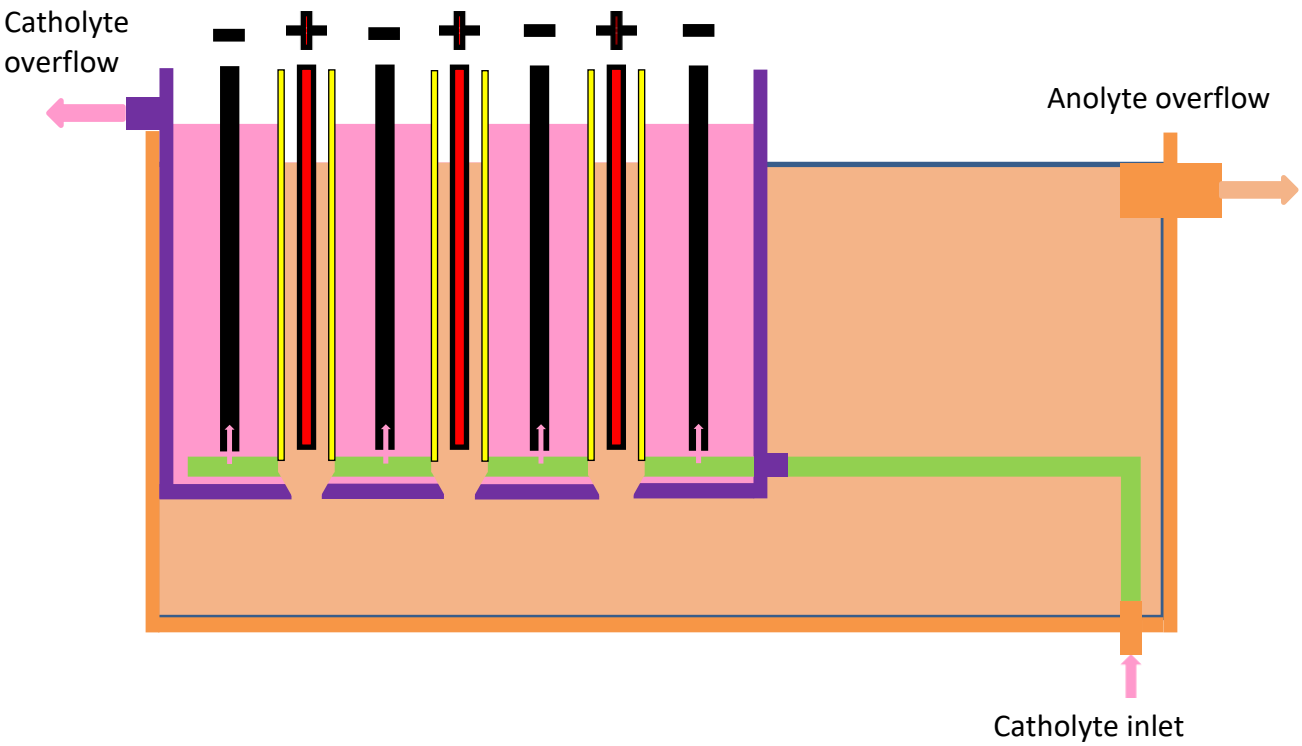

Figure 41: Cross sectional diagram of proposed cell configuration.

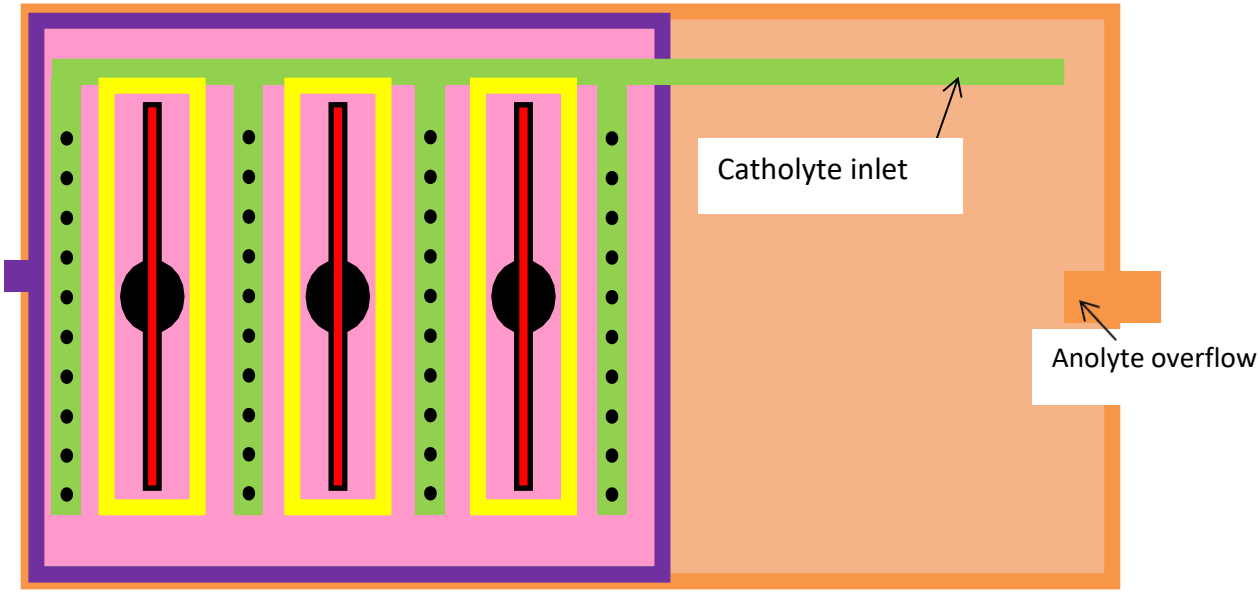

Figure 42: Top view of cell configuration, showing feed manifold (green).

4.3.3 Proposed electrodes

The cathode size is shown in Figure 43. The active area is the same as the cathodes last used for the large cell, whilst being small enough to fit in the small cell. The solution line will be ~5cm from the busbar, which will be either welded or bolted to the 1.8mm thick cathode sheet.

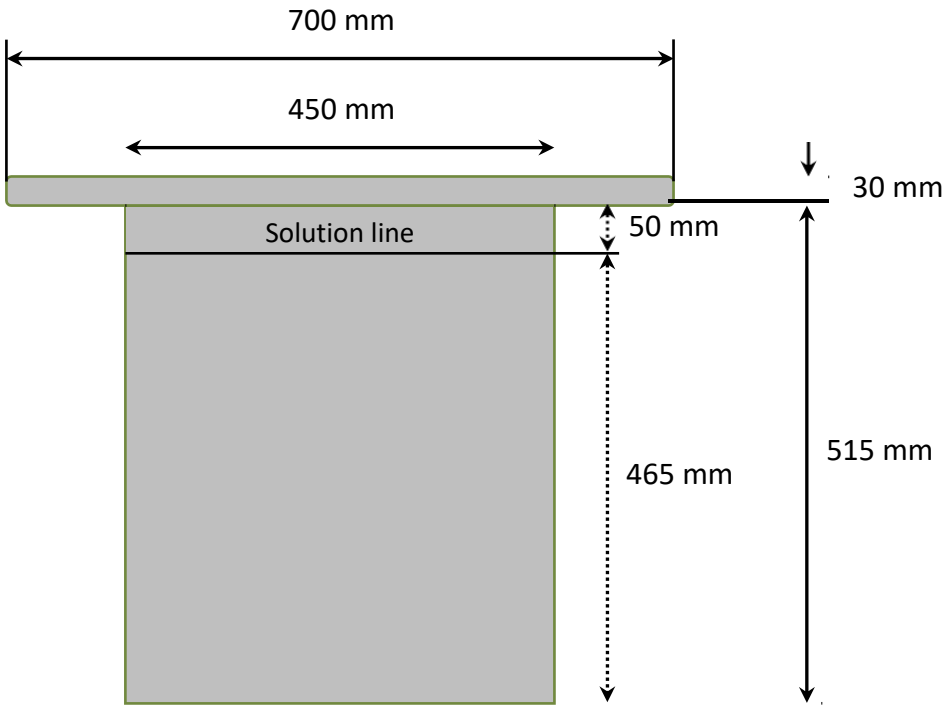

Figure 43: Cathode size for EMM EW cell

The cathode to anode ratio of 1.8 can be accomplished via multiple designs, hence there are two anode designs proposed, with the optimal one yet to be chosen. Each anode design will use Pb/Ag alloy and have a thickness of 10mm.

The first design, shown in Figure 44, has the same length, but a smaller diameter of 280mm compared to the cathode diameter of 450mm. This is the simplest of the two designs however it is possible the current density at the edges of the cathode will be less than the current density at the centre, as the anode will only be directly opposite 280mm of the 450mm wide surface.

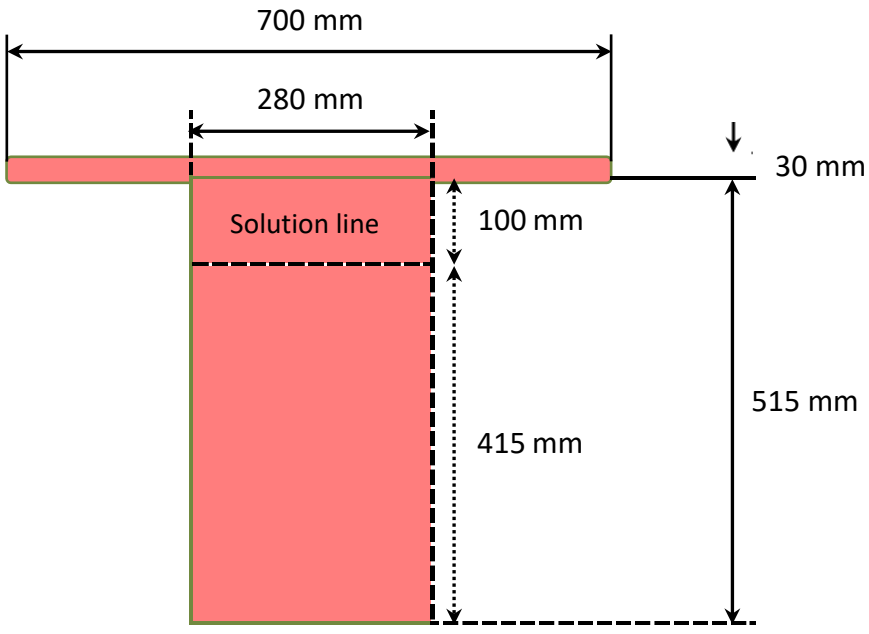

Figure 44: Anode design 1; same length and smaller width.

The second design (Figure 45) attempts to address the shortcomings of design one by sacrificing simplicity. This design has perforations of 110mm x 40mm throughout the active area. This leaves 20mm thick Pb/Ag remaining. This design should allow for more even current distribution on the cathode, however the durability and longevity of the design is not known, and suspected to be significantly less than the first design.

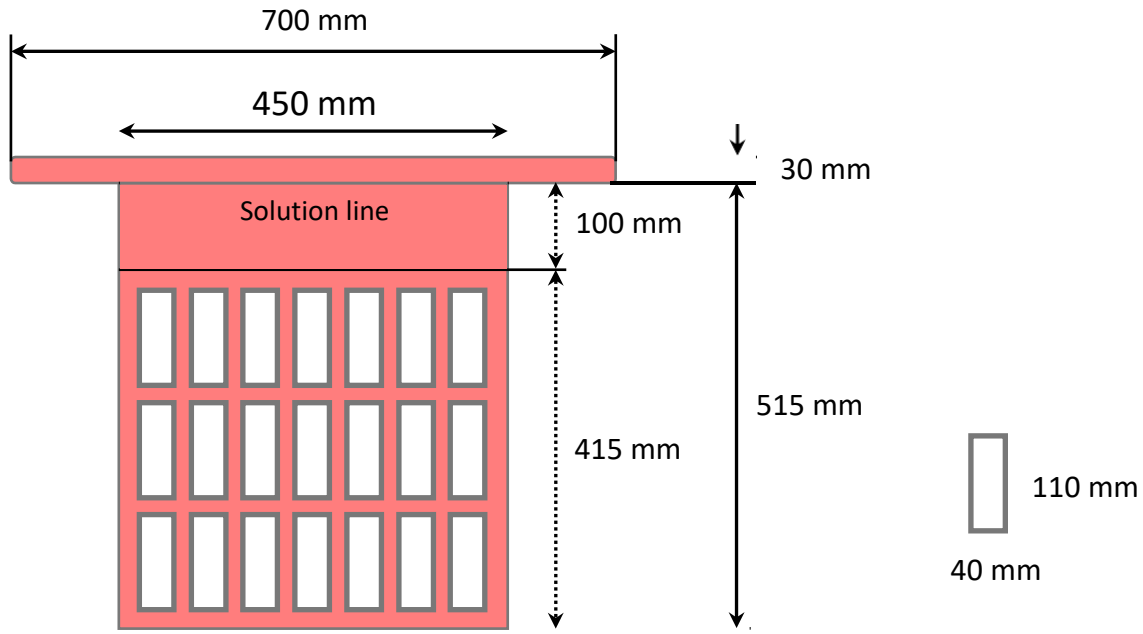

Figure 45: Anode design 2; perforated anode of the same length and width as the cathodes

4.3.4 Diaphragms

Several communications with "Clear Edge, Filtration Group Corporation" agent in Western Australia to source the diaphragm locally is ongoing. Filtration Group Corporation has a factory in Victoria – Australia. They can supply two types of diaphragm, a polypropylene (PP) cover at high permeability – 4 $m^3/m^2/min$, and a PP fabric with low permeability – 0.18 $m^3/m^2/min$. MPI will get one A4 size sample of each to be tested in our lab.

E25, mentioned in the last meeting (04FEB2020) that they will source diaphragm from China to be handed to MPI.

4.3.5 Overall electrolyte circulation

The catholyte will be circulated from the overflow back into the feed tank, which will be pumped into the feed manifold and subsequently into the cell. There will be a concentrated feed that will be added to the circulating feed to replenish the manganese as it is plated. The anolyte overflow will be collected and will not re-enter the cell. This is demonstrated in Figure 46.

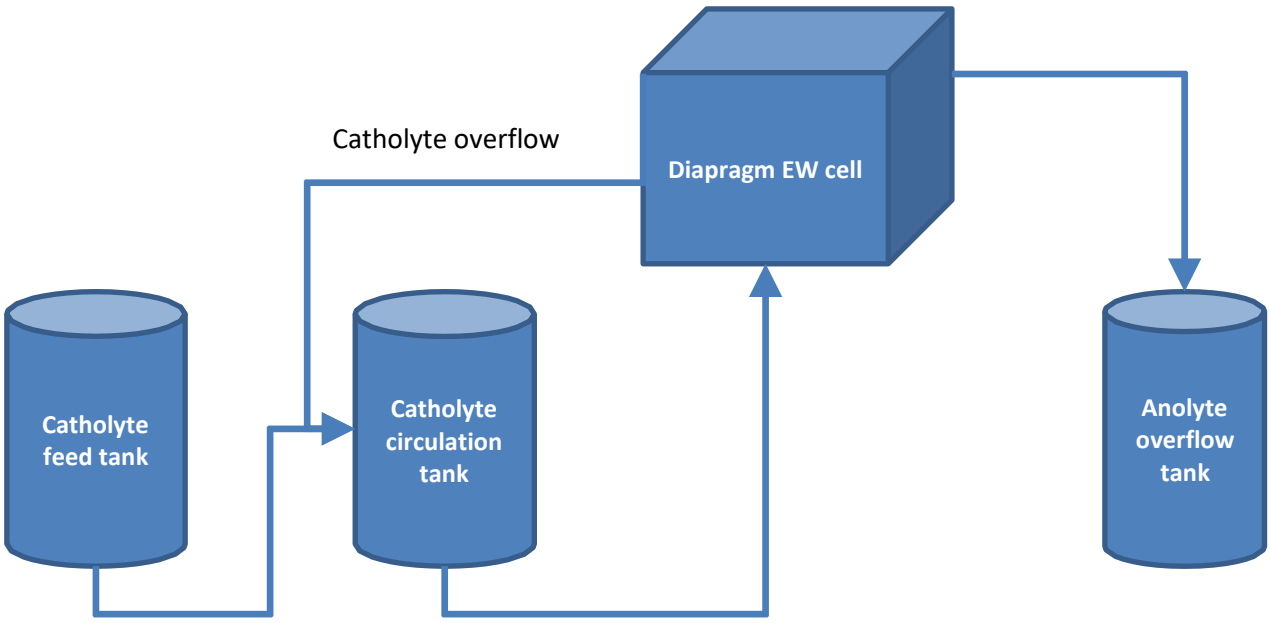

Figure 46: Overall circulation of the electrolyte of the pilot plant.

5 Conclusions

Electropolishing method is an exceptional procedure in which smooth metal surface can be obtained. Several parameters that affect the metal surface like electrolyte, current density, temperature, and potential were tested during this project. A few tests succeeded in producing shiny metal surface. During electropolishing, the colour of the electrolyte turns from colourless to a dark orange/yellow/brown, this may be due to dissolution products; possibly iron or chromium.

The data from the two electrowinning tests were consistent with the results from Phase 1 and 2, but the EMM deposit from the 24-hour electrowinning test was noticeably black around its edges especially the region nearest to the solution line. The results from the SEM-EDX characterisation of the black powdery compound appear to suggest it as some sort of oxides, possibly of manganese. This appears consistent with the results from the SEM-EDX characterisation of the black region on the metal piece. Trace amount of cobalt was picked up during the EDX analysis. Cobalt, when present above certain concentration, was demonstrated in past studies as the cause for the black appearance on the EMM deposit. It appears that a study is warranted to investigate and establish the relationship between the concentration effect of cobalt in the feed solution and the occurrence of the black powdery compound on the EMM deposit relating to the visual appearance of the EMM deposit. It may be that a substantial amount of the black powdery compound on the EMM deposit can be produced for XRD characterisation to ascertain the identity of this black powdery compound.

A full detail proposed design to modify the existing pilot plant to fit for manganese electrowinning. The proposed design included the dimensions of the EW cell and cathode and also the flow of electrolyte through the cell in its current state.

6 References

1. 25, E., *Element 25 Limited ASX release*. 2017.
2. Tailor, P.B., A. Agrawal, and S.S. Joshi, *Evolution of electrochemical finishing processes through cross innovations and modeling.* International Journal of Machine Tools and Manufacture, 2013. **66**: p. 15-36.
3. Cadien, K.C. and L. Nolan, *7 - CMP Method and Practice*, in *Handbook of Thin Film Deposition (Third Edition)*, K. Seshan, Editor. 2012, William Andrew Publishing: Oxford. p. 179-219.
4. Landolt, D., P.F. Chauvy, and O. Zinger, *Electrochemical micromachining, polishing and surface structuring of metals: fundamental aspects and new developments.* Electrochimica Acta, 2003. **48**(20): p. 3185-3201.
5. Han, W. and F. Fang, *Fundamental aspects and recent developments in electropolishing.* International Journal of Machine Tools and Manufacture, 2019. **139**: p. 1-23.
6. Mohan, S., et al., *Electropolishing of stainless steel - A review.* Transactions of the Institute of Metal Finishing, 2001. **79**: p. 140-142.
7. Landolt, D., *Fundamental aspects of electropolishing.* Electrochimica Acta, 1987. **32**: p. 1-11.
8. Yang, G., et al., *Electropolishing of surfaces: theory and applications.* Surface Engineering, 2017. **33**(2): p. 149-166.
9. Lochynski, P., et al., *Improvement of the stainless steel electropolishing process by organic additives.* 2016. **18**(4): p. 76.
10. Chen, S.C., G.C. Tu, and C.A. Huang, *The electrochemical polishing behavior of porous austenitic stainless steel (AISI 316L) in phosphoric-sulfuric mixed acids.* Surface and Coatings Technology, 2005. **200**(7): p. 2065-2071.
11. Eliaz, N. and O. Nissan, *Innovative processes for electropolishing of medical devices made of stainless steels.* Journal of Biomedical Materials Research Part A, 2007. **83A**(2): p. 546-557.
12. Haïdopoulos, M., et al., *Development of an optimized electrochemical process for subsequent coating of 316 stainless steel for stent applications.* Journal of materials science. Materials in medicine, 2006. **17**: p. 647-57.
13. ASTM, *Standard Specification for Passivation of Stainless Steels Using Electropolishing, B912-02 (2018)*. 2018, ASTM International,: West Conshohocken, PA.
14. Nazneen, F., et al., *Electropolishing of medical-grade stainless steel in preparation for surface nano-texturing.* Journal of Solid State Electrochemistry, 2012. **16**(4): p. 1389-1397.
15. Rokicki, R. and T. Hryniewicz, *Enhanced oxidation–dissolution theory of electropolishing.* Transactions of the Institute of Metal Finishing, 2012. **90**: p. 188-196(9).
16. Lochynski, P., et al., *Improvement of the stainless steel electropolishing process by organid additives.* Polish Jornal of Chemical Technology, 2016. **18**(4): p. 76 - 81.
17. Balistrieri, L.S. and T.T. Chao, *Adsorption of Se by amorphous Fe oxyhydroxide and MnO_2.* Geochimica et Cosmochimica Acta, 1990. **54**(3): p. 739-751.